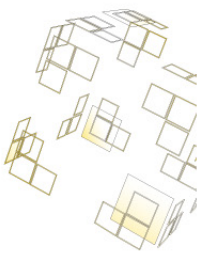
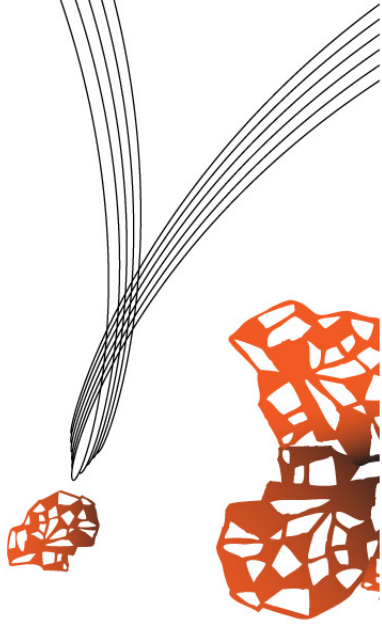


Bachelor Thesis  
Applied Physics, Faculty of Science and Technology

# Transverse Pressure Dependence of AC Coupling Losses in YBCO CORC Cables



M.A.R. Krielaart  
August 22, 2013



*Supervisors*  
dr. M.M.J. Dhallé  
MSc. P. Gao

UNIVERSITY OF TWENTE.



# PREFACE

As a final part of my bachelor education program at the University of Twente, the result is the report in front of you. How funny is it if I come to realize, that three (okay, honestly four but I enjoyed my combined last year of studying and being the chairman of the University ballroom dancing association) years of studying physics in all different fields like optics, fluids, classical mechanics and computational physics, the final assignment actually not only combines some of these topics, but actually introduced a new subject to me as well; *superconductivity*.

At one of the first days during my assignment at the EMS chair, I noticed a PhD comic about the thesis repulsor field<sup>1</sup> in one of the offices and I have to say that I think most of the phases described in that comic are also true for me.

One of the most important things that I have learned during my time doing this experiment is that it is simply not the type of experiment I was used to do. Not just putting value  $a$  on the dial of some device, reading output  $b^2$  and plotting the values  $(a, b^2)$  to see some theory that already predicted that  $a = b^2$  actually holds. During the experiments described in this report, I realized that the 'real' physics is much more in depth compared to the experiments I have done so far, which were actually more focused on learning the 'how-to' of experimenting.

I think the most important thing I learned from doing this assignment is that physics is actually the thing I'd like to continue with, other than I thought at the beginning of this project, when I more thought of it as maybe just the last assignment to get my bachelor degree. Also the topic superconductivity attracted me in such a sense, that I decided to continue my education by following a master in this direction.

None of this was made possible without the enthusiast help and support I received from my teacher, Marc Dhallé in the first place (thanks for all your patience to explain me some topics over and over again, stressing exactly those points which you noticed I didn't understand) and PhD student Peng Gao for letting me follow and be a part of his continuing study about pressure dependences in superconductors.

As a final remark, my lack of photoshop (or alike) skills forced me to adhere to the new slogan of the university, 'High tech, human touch'. It are most of the drawings in this report that represent the 'human touch' part of this slogan.

---

<sup>1</sup>See the great PhD comics website, [www.phdcomics.com/comics/archive.php?comicid=1354](http://www.phdcomics.com/comics/archive.php?comicid=1354) for the specific comic about the thesis repulsor field.



# SUMMARY

It is necessary to find a way to produce superconducting cables in such a way that the losses in alternating (AC) magnetic fields are as low as possible. One of the methods that is currently tested is the losses that occur in YBCO Conductor on Round Core (CORC) cables. In this type of cable, multiple YBCO tapes are wound around a central tube.

It is the purpose of this report to describe the effect of a transverse mechanical pressure on such cables on the coupling losses that occur for different external magnetic field frequencies, as this coupling losses are a function of frequency and pressure.

To measure the resulting coupling losses, inductive measurements have been done alongside calorimetric loss measurements. The data of the last method is, however, for further on described arguments not used in the presentation of the data in this report. Although this disables the possibility to speak about losses in absolute terms, still relative effects can be studied with this data.

It follows from the experiments that the used setup is not sensitive enough to measure any significant coupling losses. Some arguments on whether this is because the coupling losses are really small or if this is a set-up only 'problem', are discussed.



# CONTENTS

<b>1 Introduction</b>	<b>9</b>
1.1 Assignment description . . . . .	9
1.2 About superconductivity . . . . .	9
1.2.1 HTS, YBCO, CORCC . . . . .	10
1.2.2 The need for cables . . . . .	10
1.2.3 AC losses . . . . .	12
1.3 Course of the assignment and lay-out of the report . . . . .	16
<b>2 Experimental</b>	<b>17</b>
2.1 Samples . . . . .	17
2.2 AC loss set-up . . . . .	17
2.2.1 Inductive measurement method . . . . .	19
2.2.2 Calorimetric measurement method . . . . .	21
2.3 Transverse pressure insert . . . . .	21
2.3.1 1D thermal model . . . . .	21
2.3.2 COMSOL simulations . . . . .	22
2.3.3 Model validation . . . . .	23
2.4 Measurement description . . . . .	27
2.5 Data processing . . . . .	27
<b>3 Results</b>	<b>31</b>
<b>4 Discussion and recommendations</b>	<b>35</b>
4.1 Phase shift in DC differential amplifiers . . . . .	35
4.2 Power source dependence . . . . .	35
4.3 Strain gauge values . . . . .	35
4.4 Flow meter sensitivity and resolution . . . . .	36
4.5 Changing amplification factors in the course of the experiment . . . . .	36
4.6 Simulation of YBCO CORCC pressure dependence . . . . .	36
<b>Appendix A Analytical background of the data processing method</b>	<b>37</b>
A.1 Complex numbers . . . . .	37
A.2 Magnetic field . . . . .	37
A.3 Coil signals . . . . .	38
A.4 Higher harmonics of the magnetization . . . . .	39
<b>Appendix B Calculated magnetization curves and loss plots</b>	<b>41</b>
<b>Appendix C Clamp plate construction drawings</b>	<b>59</b>



# CHAPTER 1

## INTRODUCTION

### 1.1 Assignment description

This bachelor report is about the construction and testing of a new measurement set-up that allows to measure changes in the AC coupling loss in a Yttrium Barium Copper Oxide (YBCO,  $\text{YBa}_2\text{Cu}_3\text{O}_7$ ) Conductor On Round Core (CORC) cable superconductor arising from transverse pressure due to a Lorentz force on the cable.

In this chapter, first a general introduction to superconductivity will be given. This introduction describes the theory of the phenomena, in order to understand the problem at hand in this report. The main purpose of this chapter is to give understanding why superconducting cables are needed.

After this general introduction, the experimental set-up developed for this type of measurement will be described in chapter 2. This description consists of various models used for the design of the experimental holder as well a description of the sample used and the applied measurement techniques. The measured coupling losses are shown in chapter 3 (and the corresponding magnetization curves in appendix B). In chapter 4 the results are discussed.

### 1.2 About superconductivity

In this introduction, the main aspects of superconductivity that are relevant to this assignment are briefly mentioned. Interested readers are referenced to [3] for more details.

When at a sufficiently low temperature two electrons at the Fermi surface have an electron-phonon interaction and pair, the resulting combination is called a Cooper pair. The total spin of such systems is either zero or one which makes a Cooper pair behave like a boson and thus allows it to have a total energy lower than the Fermi energy.

Cooper pairs are responsible for superconducting phenomena. Within a superconductor, the electrical resistance is zero, so that a superconducting wire can carry several kilo-amperes per square  $\text{mm}^2$ .

To describe superconductors in physical terms the BJT-space is used. That is, the phenomenon only occurs for certain values of external magnetic field (B), current density (J) and temperature (T). When (material specific) critical values of  $B_c$ ,  $J_c$  or  $T_c$  are exceeded, the superconducting behavior is destroyed. An example of a critical surface is shown in figure 1.1.

Another property of superconductors is that they expel magnetic fields. This effect is called the Meissner-effect. The superconductor achieves the exclusion of external magnetic fields by means of an induced screening current at the exterior of the sample. At the first critical field  $B_{c1}$ , these screening currents cost too much kinetic energy and the material allows some magnetic flux to enter in the shape of quantized flux tubes, each surrounded by a current. This is called a vortex. As  $\mu_0 H$  increases further, more vortices enter, until finally the external field overcomes the critical field value  $B_{c2}$  of the sample and the superconducting behavior breaks down.

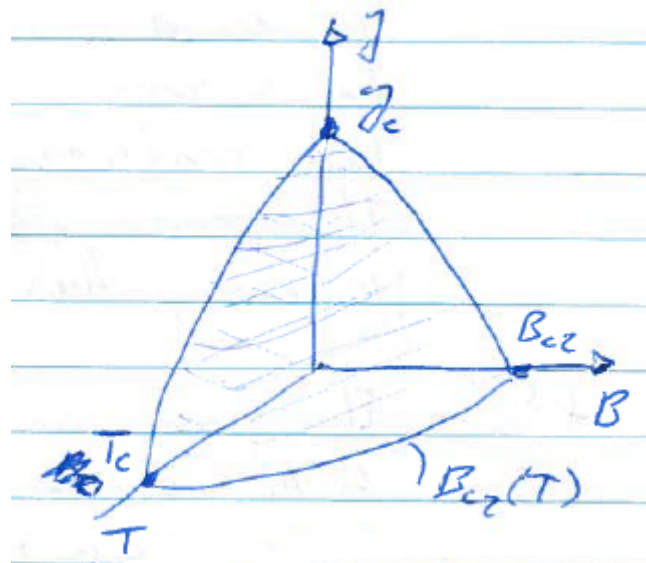


Figure 1.1: Impression of the critical surface for an arbitrary superconducting material. In literature, the  $T = 4.2\text{K}$  slice of this 3D plot is often shown, as the boiling point of helium is of the same temperature.

### 1.2.1 HTS, YBCO, CORCC

One branch of superconductors is the so called High Temperature Superconductors (HTS). The advantage of HTS compared to low temperature superconductors is that the critical temperature is higher than the boiling point of liquid nitrogen ( $T_b=77\text{K}$ ). As liquid nitrogen is easier to produce and thus less expensive in use compared to liquid helium, the advantages of HTS are easily understood.

The samples of interest for this experiment consist of YBCO, which is a high temperature superconductor. As YBCO is grown on a substrate, it is usually produced in the form of thin tapes with a typical width of a few millimeters and a height in the order of microns. The structure of YBCO is displayed in figure 1.2.

One difficulty in producing YBCO tapes is that the different crystal growth areas (grains) should be aligned well, with a maximum misalignment of the grain boundaries of only about  $4^\circ$ , as a higher misalignment leads to a large reduction in critical current density [4].

YBCO is a brittle material. This hinders the use of conventional 'bonding and twisting' methods to wind cables from it. Therefore, different approaches are currently subject to tests. One of the methods is known as Conductor on Round Core (CORC) cable. For the production of CORC cables one or more YBCO tapes are wound around a central cylindrical core.

### 1.2.2 The need for cables

To explain why the test samples consist of more than one YBCO tape twisted to form the CORC cables, one needs to realize a typical use case of the cables, as superconducting windings for a (cylindrical) coil. When simplifying this geometry, some basic estimates can be made. The reader is referred to figure 1.3 in the calculations below. For an infinite straight coil, the magnetic field inside is constant, and given by

$$B = \mu_0 N I. \quad (1.1)$$

Here  $N$  is the number of turns per unit length and  $I$  is the current through the windings. From the definition of flux

$$\Phi = \int B dA = \mu_0 N I A. \quad (1.2)$$

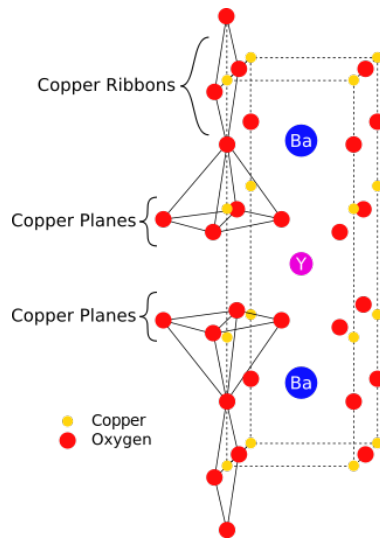


Figure 1.2: The structure of YBCO [11].

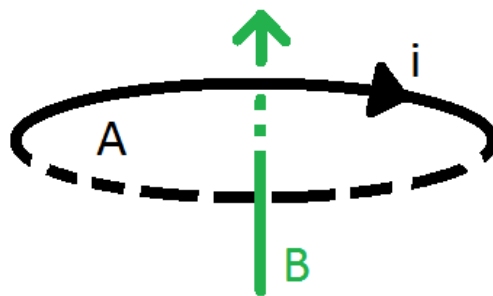


Figure 1.3: The simplified geometry of a coil winding with cross section area  $A$  carrying a current  $i$ . Inside a solenoid, the resulting field  $B$  is perpendicular to  $A$ .

The formulation of electromotive force (e.m.f.), i.e. the power (voltage) driving the system, is given by

$$\mathcal{E} = -\frac{d\Phi}{dt} = L \frac{dI}{dt}, \quad (1.3)$$

From electrical engineering, the flux through one turn is given by

$$\Phi_{1\text{turn}} = LI \Rightarrow L = \frac{\Phi}{I} \quad (1.4)$$

with  $L$  the self-inductance of the coil. From the above it can be seen that the flux per unit length is equal to

$$\Phi' = NBA = \mu_0 N^2 IA. \quad (1.5)$$

This means that the self-inductance of the coil per unit length ( $L'$ ) is proportional to the square of the number of turns per unit length ( $N$ ) given as

$$L' = \mu_0 N^2 A. \quad (1.6)$$

Since the voltage required to drive the current through the coil is proportional to  $L'$  and  $dI/dt (\propto f)$  and must be within certain constructional limits, a large self-inductance dictates a decrease in maximum frequency at which the magnet can operate. However, when many wires are combined to form a cable, with the far ends of the wires soldered together, this effectively lowers the amount of turns per unit length  $N$  and thus the self-inductance. It is for this reason that research is conducted to make cables of superconducting material, instead of single strand tapes or wires. The samples from the experiment described in this report are a new type of cable but already some success is shown using YBCO CORC cables for winding solenoidal coils [9].

### 1.2.3 AC losses

In describing superconductors, the order parameter  $\Psi$  is used, inspired by quantum mechanics. It can be shown that  $\Psi$  is proportional to  $n_s$ , the density of cooper pairs.[13].

As YBCO is a type II superconductor, magnetic field lines are able to penetrate the material. This penetration comes in the form of discrete flux quanta surrounded by current vortices. Within a vortex,  $\Psi \rightarrow 0$  reduces to zero. At the center of the vortex  $\Psi = 0$ , meaning that only normal state electrons are found in the center. This is shown in figure 1.4.

When a sample is subject to an alternating magnetic field these vortices start to move, which causes dissipation. This movement is described macroscopically by flux variation in a stationary point in space, when the magnetic field is not constant. The flux results in an electromotive force (e.m.f.) which in turn accelerates the electrons in the center of a vortex. In order to reduce this so called 'pinning' vortices, some non-superconducting impurities may intentionally be added to the sample, acting as pinning centers [10]. The interaction between the pinning center and the normal state electrons at the center of the vortex creates an energetically more favorable situation compared to a situation where the two non-superconducting centers are not overlapping.

Flux flow does not occur at all values for the magnetic field and temperature. Only for certain values of  $B$  below  $B_{cq}(T)$  pinning will occur. A schematic representation of this is displayed in figure 1.5.

Another origin of losses are 'coupling' losses. This type of loss occurs due to current crossing over between adjacent YBCO tapes. The AC loss due to the motion of vortices is called 'hysteresis' loss [6]. This crossover has a certain electrical resistance and therefore energy is dissipated. When multiple layers of YBCO tapes are stacked on top of each other as done in CORC cables one can distinguish two types of resistance. One type is the adjacent resistance  $R_a$  whereas the other type is called cross-over resistance  $R_c$ . These resistances are also shown in figure 1.6 for the case of stacked tapes.

For the purpose of this report the loss of the YBCO CORC cables are determined under various values of force in the transverse direction of the cable. As a higher force pushes the stacked filaments closer together, it is expected that the cross-over resistance reduces, thus resulting in a higher dissipation.

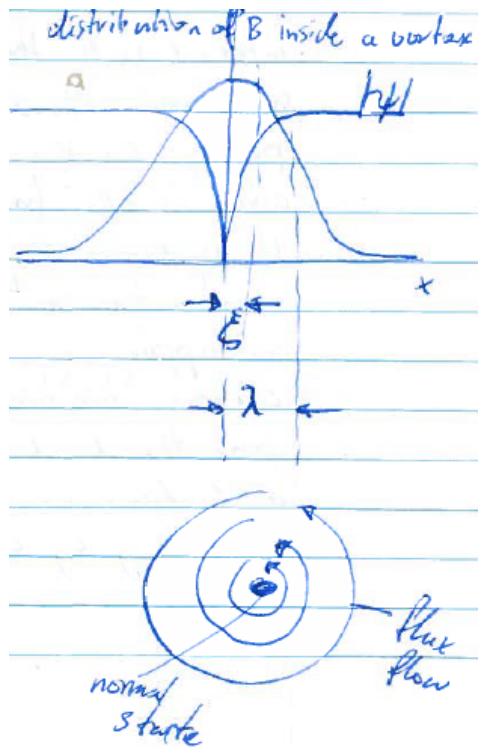


Figure 1.4: Distribution of the magnetic field  $B$  inside a vortex (Gaussian line) and the state parameter  $\Psi$  which gives the density of superconducting states ( $n_s$ ).

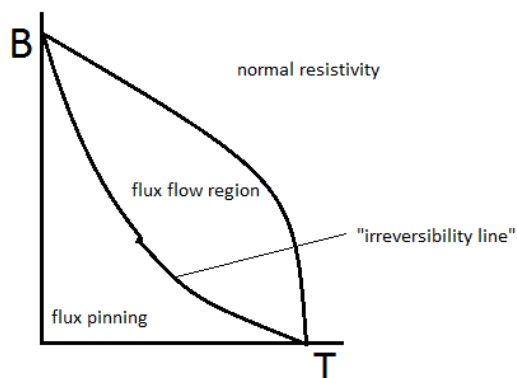


Figure 1.5: Schematic presentation of the flux flow region.

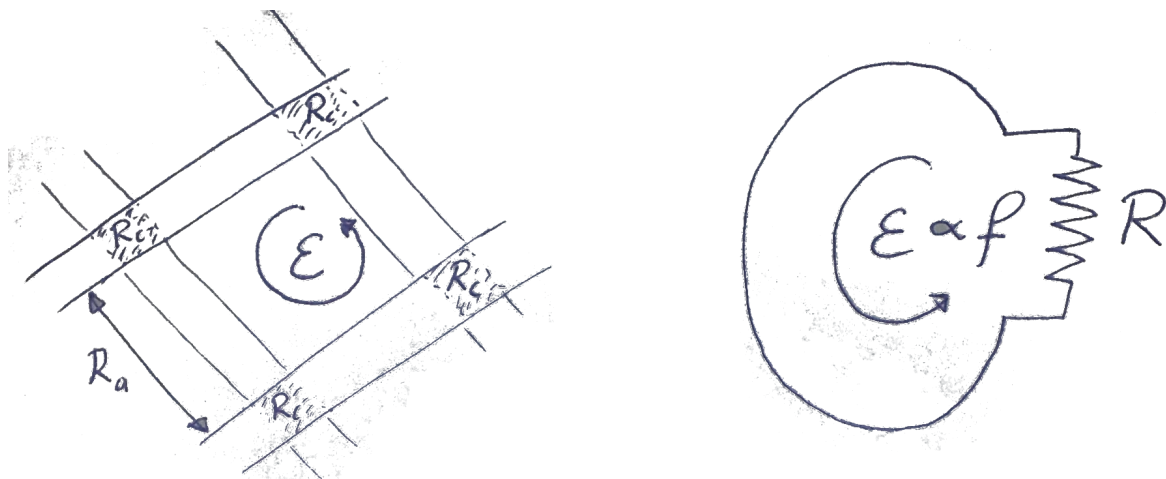


Figure 1.6: *Left*: Crossing and adjacent tapes, with the two types of distinguishable types of resistance  $R_a$  and  $R_c$ . *Right*: The simplified 'antenna' loop with a single resistance.

To verify this expectation, it is needed to separate the coupling losses from the hysteresis loss. This can be done by measuring the frequency dependence of the AC loss. Hysteresis loss is due to the movement of vortices in and out of the sample. This process is relatively fast and at practical all frequencies, the energy loss *per cycle* is expected to be frequency independent [3].

The coupling loss, on the other hand, is due to induced currents flowing between tapes and for this loss mechanism, the loss per cycle should increase linearly with frequency [3]. To understand this, the geometry on the left in figure 1.6 can be simplified further and represent the current loop as an 'antenna' closed with a normal resistor as in the right in figure 1.6. The induced electrical field in this loop will be proportional to the rate of the flux change through it and will therefore increase linearly with frequency.<sup>1</sup> Since the tapes themselves are superconducting, the electrical field in them is zero and the whole induced e.m.f. ( $\mathcal{E}$ ) drops across the normal contact resistance  $R$ . The power dissipated in this resistance is therefore  $P = \frac{\mathcal{E}^2}{R} \propto \frac{f^2}{R}$ . Expressed in loss per cycle, this gives  $P = Q_c f$ , so that  $Q_c \propto \frac{f}{R}$ .

Summarizing, the hysteresis loss *per cycle* will be independent of frequency, while the coupling loss will increase linearly with the frequency  $f$ . When the total loss is measured as a function of frequency, it is therefore expected to find a curve as in figure 1.7: a straight line with an intercept at  $f = 0$  that corresponds to the hysteresis loss and a slope indicative of the coupling loss.

<sup>1</sup>The e.m.f. also increases with the amplitude of the applied field and the area of the loop, but this is less relevant in this context.

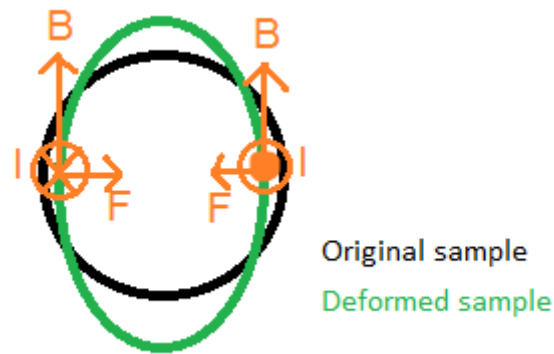


Figure 1.8: Deformation of the cross section of a YBCO CORC cable resulting from Lorentz forces on the cable.

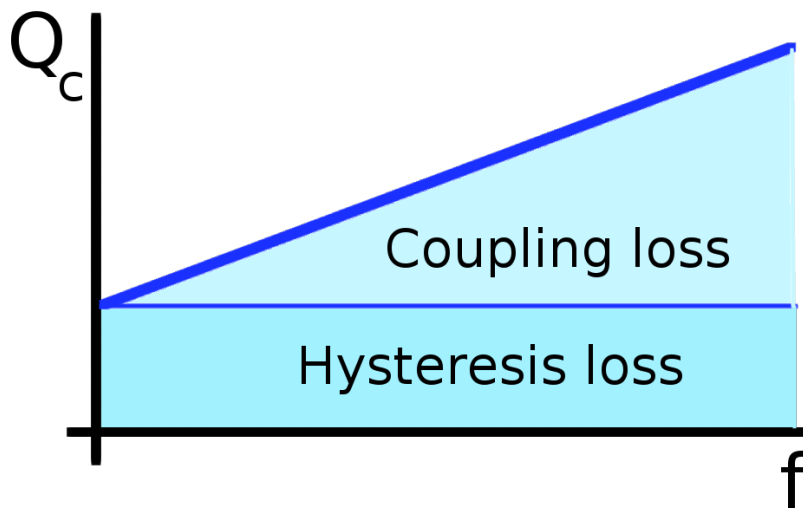


Figure 1.7: The division of the total AC loss in frequency independent (hysteresis) loss and frequency dependent (coupling) loss.

Note that if the contact resistance is decreased (e.g. by applying transverse pressure and pushing the tapes together), the contact resistance decreases and hence the coupling losses should increase as function of frequency. Hence, the slope of the curve should go up. When decreasing the pressure, the reverse process should take place.

In an application transverse pressure comes from the Lorentz force. When a magnetic field and an electrical current meet at a certain non-zero angle, the resulting Lorentz force  $\mathbf{F}$  will point in a direction defined by the cross product of the field and current:  $\mathbf{F} = q(\mathbf{E} + \mathbf{v} \times \mathbf{B})$  with  $q$  the charge,  $\mathbf{v}$  the direction of the screening currents and  $\mathbf{B}$  the direction of the magnetic field. As the screening currents are expected to roughly flow in the longitudinal direction of the cable, it is then easily seen that an alternating external magnetic field will result in a Lorentz force which is perpendicular to the wire as well, pointing inwards.

For practical applications of the samples that are tested for this report, the pressure on a sample resulting from this force may be in the order of megapascals. This means that the wire will be compressed much more in one direction on a cross section compared to other directions, as indicated by figure 1.8.

To investigate the effects of a non-uniform mechanical pressure distribution to the AC- and coupling losses on a YBCO CORC cable, a new measurement set-up is designed which clamps the sample in such a way to simulate the effects of the Lorentz force. This way, the effects of the Lorentz force on the AC- and coupling losses can be determined without actually applying a transport current to the wire as well.

### **1.3 Course of the assignment and lay-out of the report**

The assignment was formulated and carried out in the EMS chair at the University of Twente, under tutoring of the PhD student P. Gao and supervision of teacher M. Dhallé. Applied superconductivity is one of the core research areas of this chair and they are presently investigating High Temperature Superconducting (HTS) cables for various applications.

One of the detailed research questions involves the influence of the transverse pressure on the coupling losses in CORC cables and the group wanted to set up a straightforward experiment allowing to make a first assessment of this effect.

Prior to the assignment it was already decided to use a 'passive' set-up, in which transverse pressure is applied largely due to differential thermal contraction in the sample holder assembly. The assignment took the form of 1) to assist in the design and construction of this dedicated sample holder; 2) to assist in the first measurements with this insert, using an existing AC loss measurement set-up; and 3) to process the resulting data in order to gauge the influence of pressure on the coupling loss in a typical CORC cable sample.

The lay-out of this report largely reflects this chronological course of the assignment. Chapter 2 gives a brief description of the samples and the existing set-up and next focusses on the design and the realization of the transverse pressure insert. It closes with a brief description of the data processing steps, which are discussed in more detail in appendix A. Chapter 3 presents a summary of the measured data. More detail of the measured data is further shown in appendix B. In chapter 4, a general conclusion is argued with respect to the underlying research question and a number of observations are made regarding the suitability of the realized experiment and the scope for improvement.

# CHAPTER 2

## EXPERIMENTAL

This chapter describes the samples (section 2.1), introduces a few definitions and the used measurement techniques (section 2.2). The core of this chapter is concerned with the design, construction and testing of the transverse pressure insert (section 2.3). Finally, in the data processing method is elaborated (section 2.5).

### 2.1 Samples

The samples used in the experiments are YBCO tapes wound around a central tube to form CORC cables. The inner tube of the cable is made from stainless steel SS304 with an outer diameter of 4.7mm and a wall thickness of 0.8mm. Each sample is approximately 20 centimeters long. During the measurements, only the middle 12.5 centimeters (equal to the length of the clamp) are included in the detection coils, to avoid end effects (see section 2.3 setup for more details).

The samples are manufactured by Advanced Conductor Technologies in Boulder, Colorado. Seven different samples are supplied. This report only elaborates on the data of the largest sample, consisting of 39 tapes which are stacked in several layers in a fashion of  $4 \times 3 + 3 \times 4 + 3 \times 5$  tapes. The outside diameter of the cross section of the sample is 8,5mm. The cross section of a similar 24 tape CORC cable is shown in figure 2.1.



Figure 2.1: Cross section of a YBCO CORC cable. The stainless steel core around which the YBCO is wound is not displayed.

### 2.2 AC loss set-up

The sample holder consists of two stainless steel rectangular plates in which between the sample will be positioned. As discussed further in section 2.3 the two plates with the sample in between are pressed

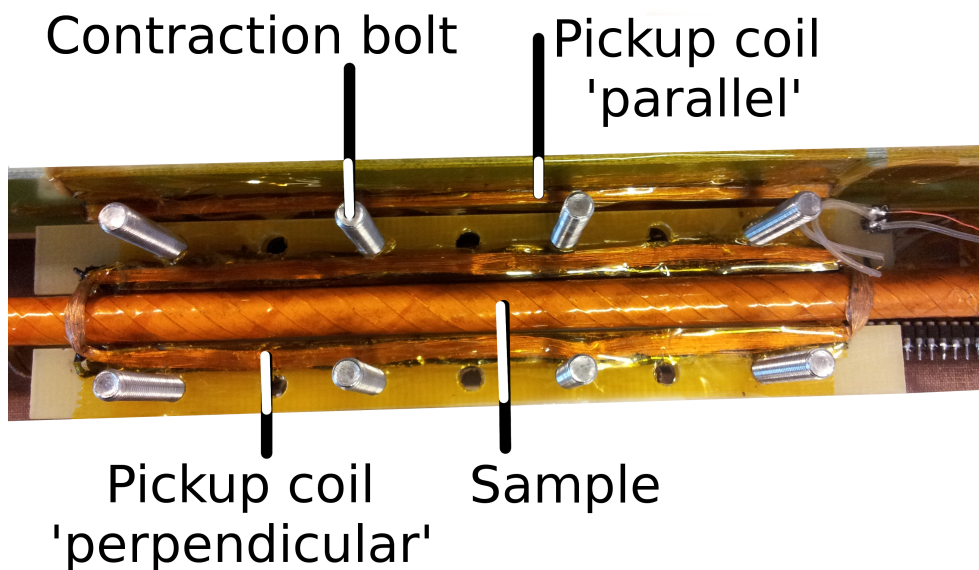


Figure 2.2: The opened clamp holding the measured sample. The pickup coil for the perpendicular measurement direction is directly on top of the sample. Also one long side of the pickup coil for the parallel measurement direction can be seen in this figure, just 'above' the first row of bolts.

together using stainless steel bolts and nuts and sets of five titanium rings per bolt. This way, the Lorentz force that would normally occur when a super current is flowing through the sample, is simulated. The specific use of five titanium rings follows from the difference in thermal contraction coefficient between stainless steel and titanium (also see section 2.3.1). As the set-up cools down, the stainless steel will contract more than the titanium, which results in a larger stress on the sample. A thin sheet of Teflon is placed between the clamp plates and the sample to avoid local extreme values in the applied force.

A pickup coil is positioned close to the sample. This positioning is achieved by winding a coil on a tube which is just greater than the thickest sample. During winding this coil is impregnated with an epoxy which is allowed to harden. Next, the long sides of this coil are glued on a G10 plate which fits between the two clamp plates. One of the clamps is attached to a insert base plate using four tapped bolts. At the far end of this base plate, the compensation coil for the pickup coil located in between the clamp plates is positioned. Figures 2.2 and 2.3 show the positioning of this pickup coil as well as the layout of the stainless steel clamps.

Perpendicular to this plate another large holder plate is constructed on where two extra coils are glued (using stycast). The coils are at the same longitudinal position on the plate as the parallel coils described earlier and permit to measure the component of the magnetic moment of the sample perpendicular to the applied pressure.

This set-up is held together at the far ends by a circular disk. Around this disk a covering tube is mounted, which is required for the calorimetric measurements (see section 2.2.2).

The measurement of the AC losses is conducted in two distinct ways but under the same conditions. By measuring in two different ways, the results of the measurements will be more reliable.

One of the measurement techniques relies on the magnetization of the sample due to the presence of an external magnetic field. This method is called an inductive measurement. The other method relies on the amount of helium that is evaporated by the dissipated heat in the system, which is called a

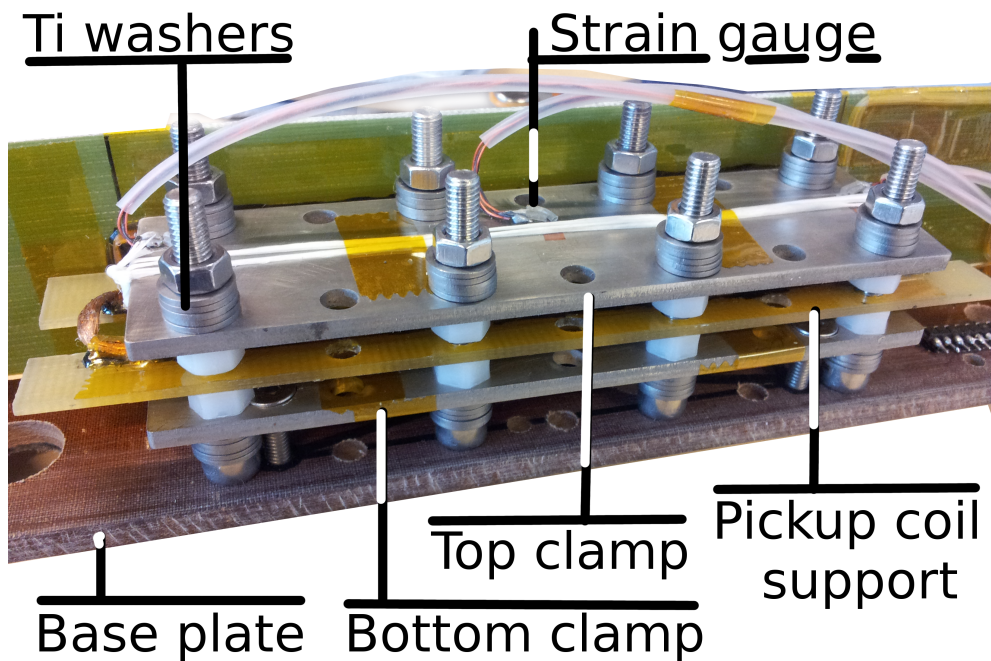


Figure 2.3: The closed clamp without a sample. The white teflon nuts are not present when a sample is inserted. The wires connected on the top clamp plate are connected to three distinct strain gauges.

calorimetric experiment.

As explained in the next paragraph and in appendix A, the inductive technique is more sensitive but requires careful data processing and relatively uncertain calibration factors. Calorimetric data, on the other hand, are less sensitive but straightforwardly calibrated. Simultaneous measurement using both techniques allows to combine the strong points of each method.

## 2.2.1 Inductive measurement method

The inductive measurement technique is based on a so called pickup coil that is placed near the sample and a compensation coil that is positioned far away from the sample, in the homogenous part of the external magnetic field and with the same size and orientation as the pickup coil. A schematic overview of this measurement technique is shown in figure 2.4.

As the sample gets subjected to the external field  $\mu_0 H$ , it starts to behave like a superconducting magnet itself. This means that the external field will give rise to a magnetic moment per volume  $M$  inside the sample. As the total magnetic induction  $B$  is given by  $B = \mu_0(H + M)$  this means that the pickup coil will measure a different value of  $B$  compared to the compensation coil far away from the sample, as the area enclosed by the compensation coil does not contain any magnetized material. That is, far away from the sample, the measured induction  $B = \mu_0 H$ . When subtracting the two signals from the coils with a differential amplifier, the resulting signal gives a measure for the magnetization as function of external field (see appendix A). It can then be shown that the loss per cycle of alternating magnetic field is given by the area enclosed by the measured magnetization ( $M$ - $B$ ) curve,  $Q_{\text{loss}} = \oint M dH$ .

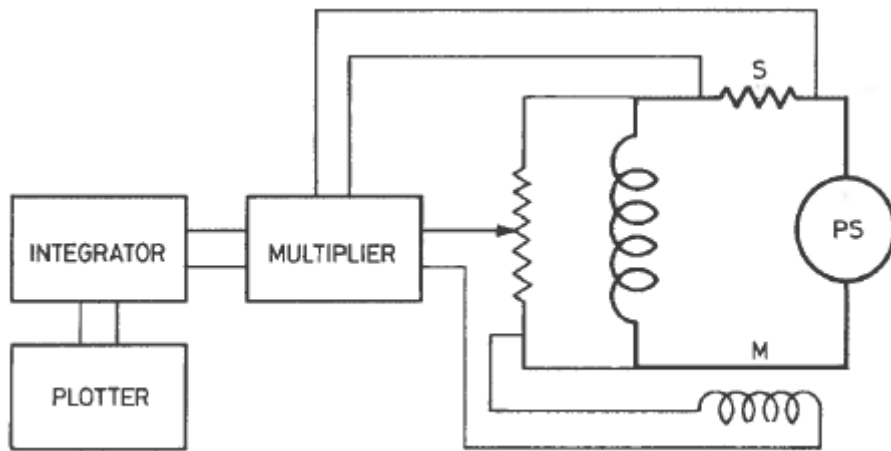


Figure 2.4: Schematic overview of the inductive measurement method [10].

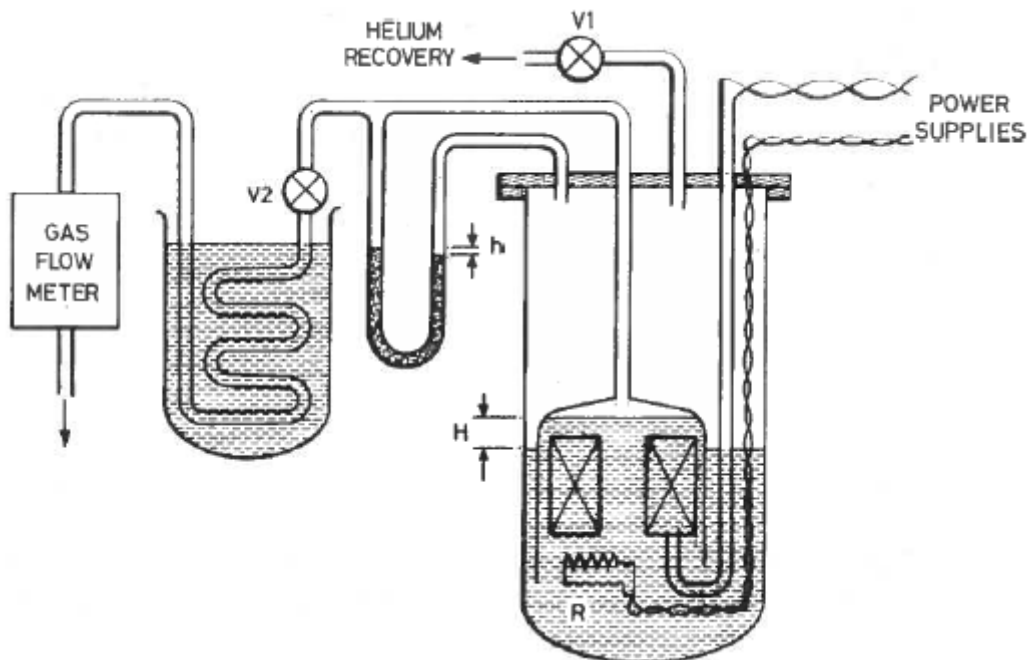


Figure 2.5: Schematic overview of the calorimetric measurement method [10].

## 2.2.2 Calorimetric measurement method

In the calorimetric measurement the evaporated helium (due to the dissipation in the sample) is measured outside of the cryostat with a (digital) gas flow meter. For a calibration, the amount of evaporated helium without an external field is measured first (heat losses due to keeping the set-up cool). After this stabilizes, an electric heater (resistor) is used to add an additionally controlled amount of heat into the vacuum, thus calibrating the flow meter. This type of measurements enables to translate losses determined with the coils, which are difficult to calibrate, to absolute losses expressed in SI-units. The system is shown schematically in figure 2.5.

## 2.3 Transverse pressure insert

### 2.3.1 1D thermal model

When cooling down the sample holder, some thermal contraction effects will occur. As the thin Teflon layer between the clamp plate and the sample will contract more than the stainless steel plate, nuts and bolts, the effective transverse stress on the sample would normally reduce when the setup is cooled down. The use of Ti washers reverts this situation causing the stress to build up.<sup>1</sup>

In order to determine the relation between the force applied on the clamp at room temperature (using the nuts) and the stress on the sample in liquid helium at 4.2K, a 1 dimensional thermal model is developed. In this model, the effects of cooling down several stacked materials with different thermal properties which are in some way restrained are described using straightforward force balance arguments. To relate the force with the nuts to the stress on the sample and also the strain measured on the top of the clamp plate, the classical bent beam model is used (see for instance [12]).

From this model, it follows that the use of sets of five stacked titanium (TiAlV) washers between the clamp plate and each end of the bolts should be used (also seen in figure 2.3). As when cooling down the sample the strain variation of the stainless steel is -0.28%, the strain on the thin Teflon (PTFE) strip is -1.6% and the strain variation of the set of titanium washers is -0.15%, it can be seen from these numbers that the relative higher contraction of the steel compared to the titanium makes the rings exert an increasing stress on the plate.

Since this effect takes place on both plates, the resulting stress on the sample will increase. Note that, for the effect of the use of the titanium washers to work, the height of the stack should be sufficiently high compared to the thickness of the Teflon strip. All mentioned values are also tabulated in table 2.1.

Material	Thermal contraction $\epsilon_T$ (%)
Stainless steel plate	-0.28
PTFE (Teflon)	-1.6
Titanium (TiAlV)	-0.15

Table 2.1: Listing of the values of thermal contraction of the different materials used in the clamp design.

Prior to cool-down, the sample is pre-stressed at room temperature with 3 strain gauges and the stress is measured as a deformation of the clamp plates. The 1D model estimates the build up of stress between room temperature and 4.2K, but cannot predict the deformation of the clamp plates. For this, the analytical bent beam expression is used. However, since the plates have a non-uniform cross section, its predictions are double checked with a 2D COMSOL model. The COMSOL model also allows to estimate the contact stress between the Teflon and the clamp plate on the one hand, and the Teflon and the sample on the other.

<sup>1</sup>The Ti has the lowest thermal contraction coefficient and thus effectively (i.e. relative to the other materials) 'expands' upon cooling down, putting also the other components under compression.

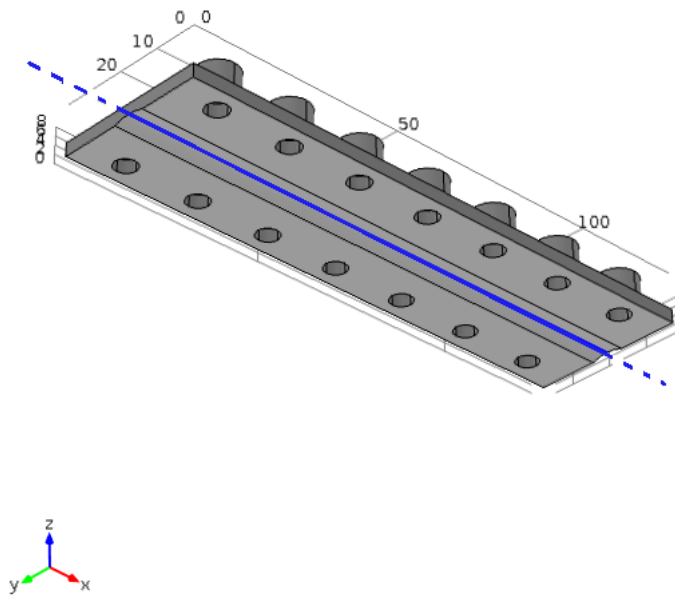


Figure 2.6: The (dashed) blue line indicated the line of fixed constraint (A-A) in the 3D model geometry.

### 2.3.2 COMSOL simulations

To verify the 1D thermal model, a 2D model is build using COMSOL. In this model, a cross section of the setup is modeled. With the data resulting from this model, the relation between the applied force on the plate and the stress on the sample, as well as the strain on the top of the clamp plate are determined.

Besides the 2D model a less detailed 3D model is build using COMSOL. In this model, the dimensions of the real clamp are used as indicated in figure C.1. To make a more realistic model, the applied boundary load which in the real model is applied via the titanium nuts, is not simulated immediately on the clamp surface, but via a stack of five M5 nuts.

To simulate the presence of the sample, the centerline of the gutter is assumed to be fixed, i.e. it is not able to move in space during the calculation time. This model is less realistic than a model that actually simulates the sample underneath the gutter (as in the 2D model), but by making the area of fixed constraint as thin as possible, it is expected that the result will not vary widely from a simulation including a modeled sample as well. The line of fixed constraint is displayed in figure 2.6.

The property of interest in this case is the  $yy$ -component of the strain tensor ( $\epsilon_{yy}$ ). In figure 2.7, this component is displayed using a false color map, with red indicating high strain components in the  $y$  direction while dark blue colors indicate low values of strain. Note that in the figure, only the positive components are shown, all negative strains are not specified in the display, as these arise at the bottom of the clamp only.

Data from the 3D model are extracted in two ways. On way is taking the strain value approximately at the three points that are also measured on the real clamp plate. Another method determines the average over the entire centerline of the clamp plate. For both methods data is presented in section 2.3.3.

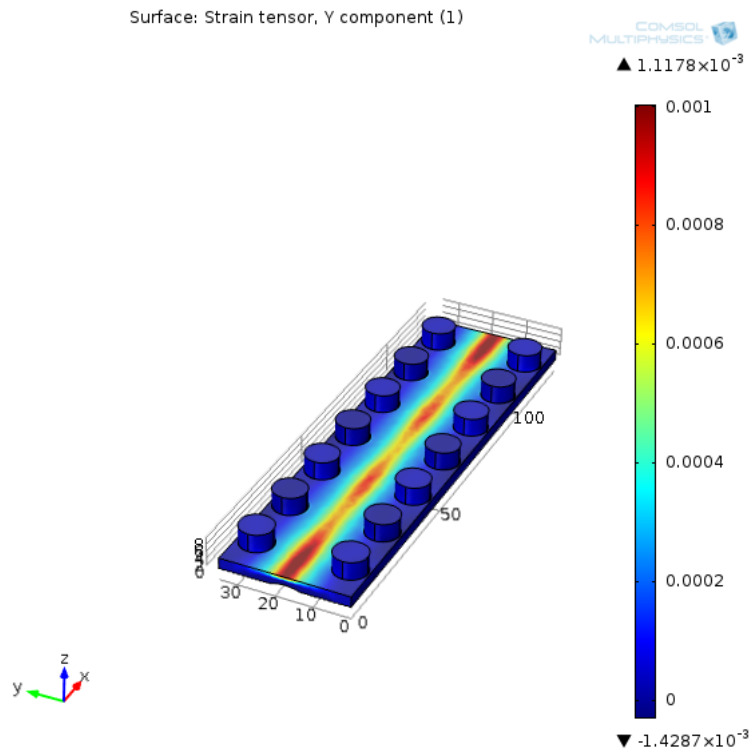


Figure 2.7: Simulation of the strain in the y direction for a total applied force  $F_T = 3.4\text{kN}$ .

### 2.3.3 Model validation

To validate the COMSOL models, a Teflon tube with a radius of 7,5 millimeters (approximately the radius of the thickest sample) is placed between the clamp plates. The three strain gauges are next attached to two distinct Keithley 196 and one 199 multimeter devices. To accurately measure the strain at the top of the clamp with the strain gauges, a 4-wire resistance measurement is done. In this type of resistance measurements, 4 wires per strain gauge are used to measure the resistance. These wires are connected as close as possible to the two strain gauge connectors. This type of measurement is used because the change in resistance during the measurement will be small, in the order of 1/10000 of ohms. By using this method, one measures the actual voltage drop across the strain gauge, instead of also the voltage drop across the cables of a standard 2 point measurement. The schematic process of a 4-wire resistance measurement is shown in figure 2.8.

During the validation, bolts are tightened on the first, third, fifth and seventh set of holes in the clamp plates. For different torques of the nuts the strains are measured. The associated force is calculated using classical bend beam model and relations between torque and force for M5 nuts and bolts from the poly-technical handbook [1]. An average of the three strain values is calculated afterwards and compared to the average of the COMSOL models.

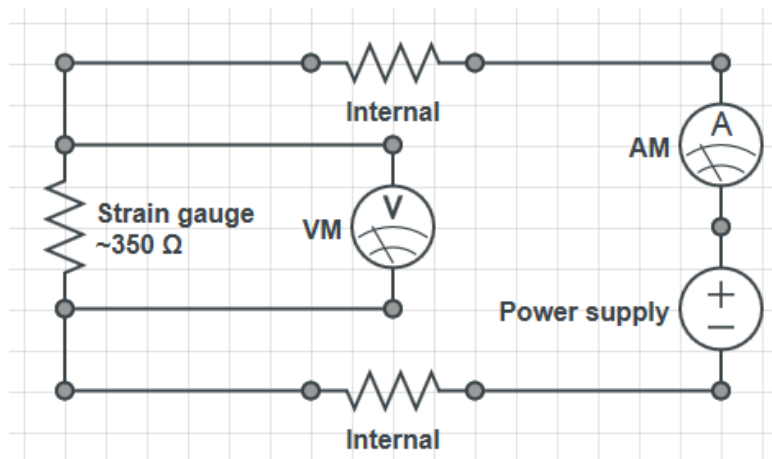


Figure 2.8: Schematic overview of a  $\Omega$ 4-wire measurement.

$R_5(\Omega)$	$R_6(\Omega)$	$R_7(\Omega)$	$\epsilon_5(\%)$	$\epsilon_6(\%)$	$\epsilon_7(\%)$	Average $\epsilon(\%)$	Total force (N)
350,316	350,779	350,51	0	0	0	000,0E+0	000,0E+0
350,323	350,938	350,46	9,52E-04	2,16E-02	-6,79E-03	5,2E-3	224,9E+0
350,327	350,961	350,415	1,50E-03	2,47E-02	-1,29E-02	4,4E-3	189,9E+0
350,408	351,039	350,474	1,25E-02	3,53E-02	-4,89E-03	14,3E-3	613,0E+0
350,494	351,102	350,563	2,42E-02	4,38E-02	7,20E-03	25,1E-3	1,1E+3
350,562	351,178	350,618	3,34E-02	5,42E-02	1,47E-02	34,1E-3	1,5E+3
350,627	351,211	350,653	4,23E-02	5,86E-02	1,94E-02	40,1E-3	1,7E+3
350,728	351,339	350,78	5,60E-02	7,60E-02	3,67E-02	56,2E-3	2,4E+3
350,832	351,432	350,774	7,01E-02	8,86E-02	3,59E-02	64,9E-3	2,8E+3
350,967	351,495	350,882	8,85E-02	9,72E-02	5,05E-02	78,7E-3	3,4E+3
351,049	351,559	351,048	9,96E-02	1,06E-01	7,31E-02	92,9E-3	4,0E+3
351,189	351,682	351,054	1,19E-01	1,23E-01	7,39E-02	105,1E-3	4,5E+3
351,187	351,787	351,131	1,18E-01	1,37E-01	8,44E-02	113,2E-3	4,9E+3

Table 2.2: Measured resistance as function of applied force with the three strain gauges (numbered 5, 6, 7). Also the calculated strain is displayed in percent.

In table 2.2 the results are displayed. The average value of the strain determined from the measurement and the simulations for the different applied forces is plotted in figure 2.9.

To get a clear view of the accuracy of the computer models, the relative errors between the outcome of the various computer models and the 4-wire resistance measurement are calculated. The result is shown in figure 2.10. From this it can be seen that the three different models vary in the relative error.

The most accurate method ( $\sim 6\%$  deviation from the measurement results) is also the most resource intensive simulation as this is the simulation in which the clamp is modeled in 3D. From the resulting dataset, an average is then computed along the top of the A-A section (see figure 2.6).

To some surprise the 2D model is the next most accurate model to predict the measured strain. The error is on average not more than twice as large compared to the 3D line average model, and has the advantage of being less resource intensive for simulation. The results from the three point measurement of the 3D model vary most from the actual measured value. When having a look at the graph which shows the variation of the strain on the top of the A-A section, this might be explained by the local extreme values that occur at the point of measurement. One simulation outcome is displayed figure 2.11).

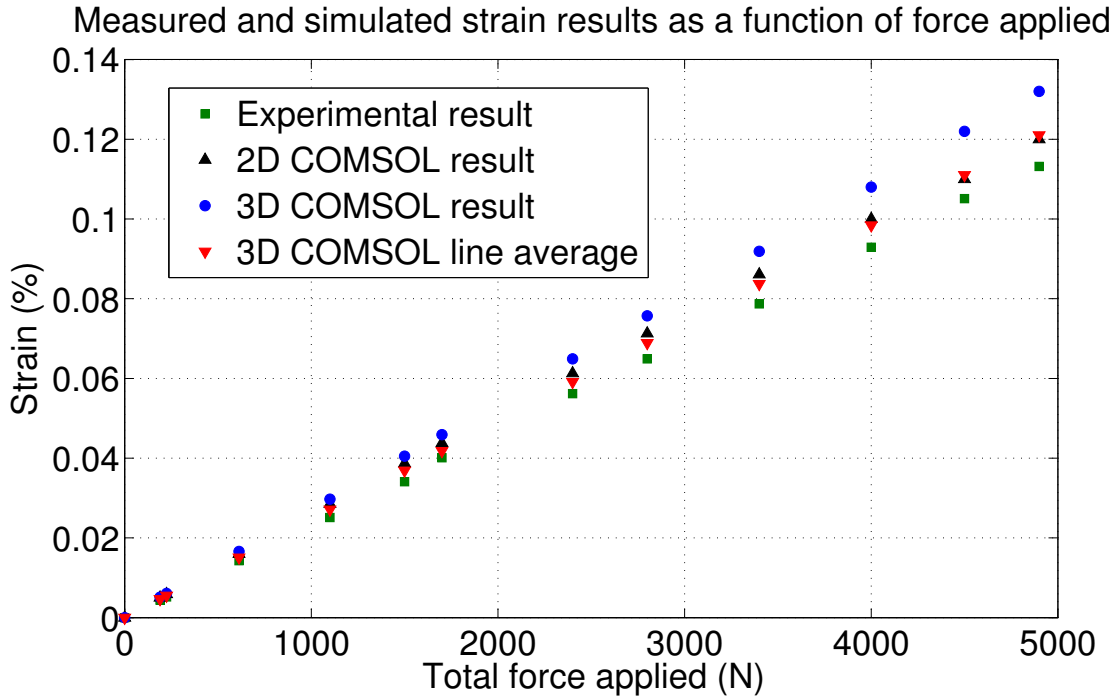


Figure 2.9: Comparison of the measured and simulated strains on the top clamp plate.

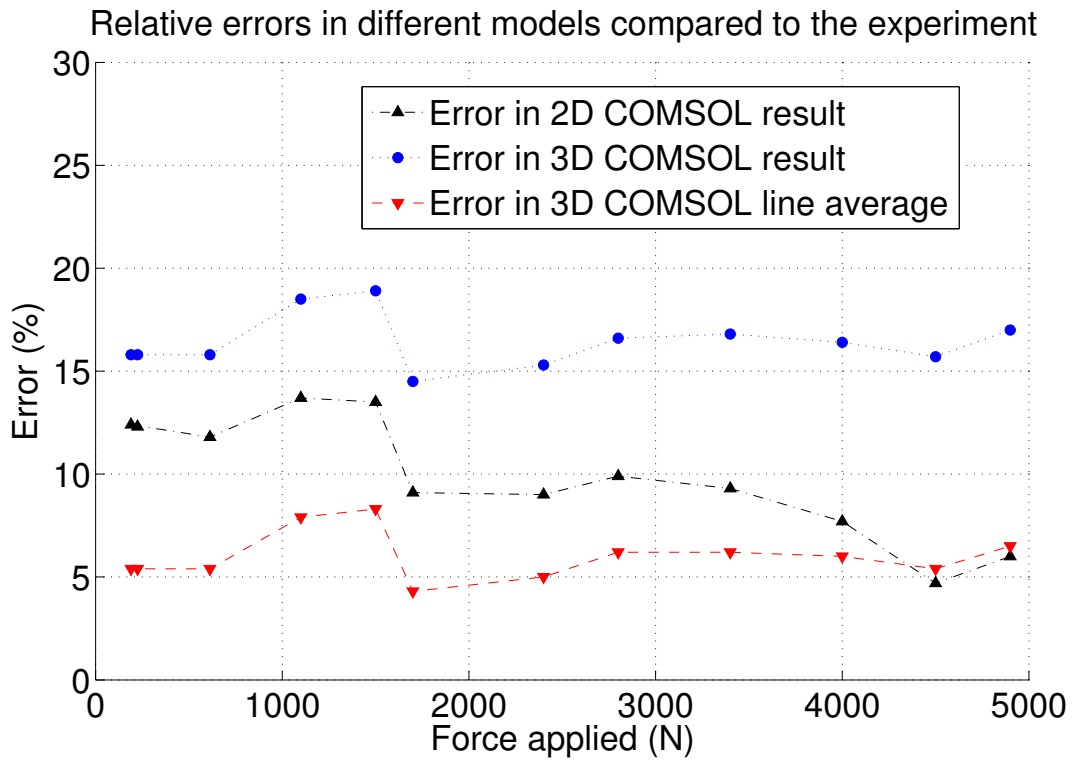


Figure 2.10: The relative error between the strain measurement and the different simulations.

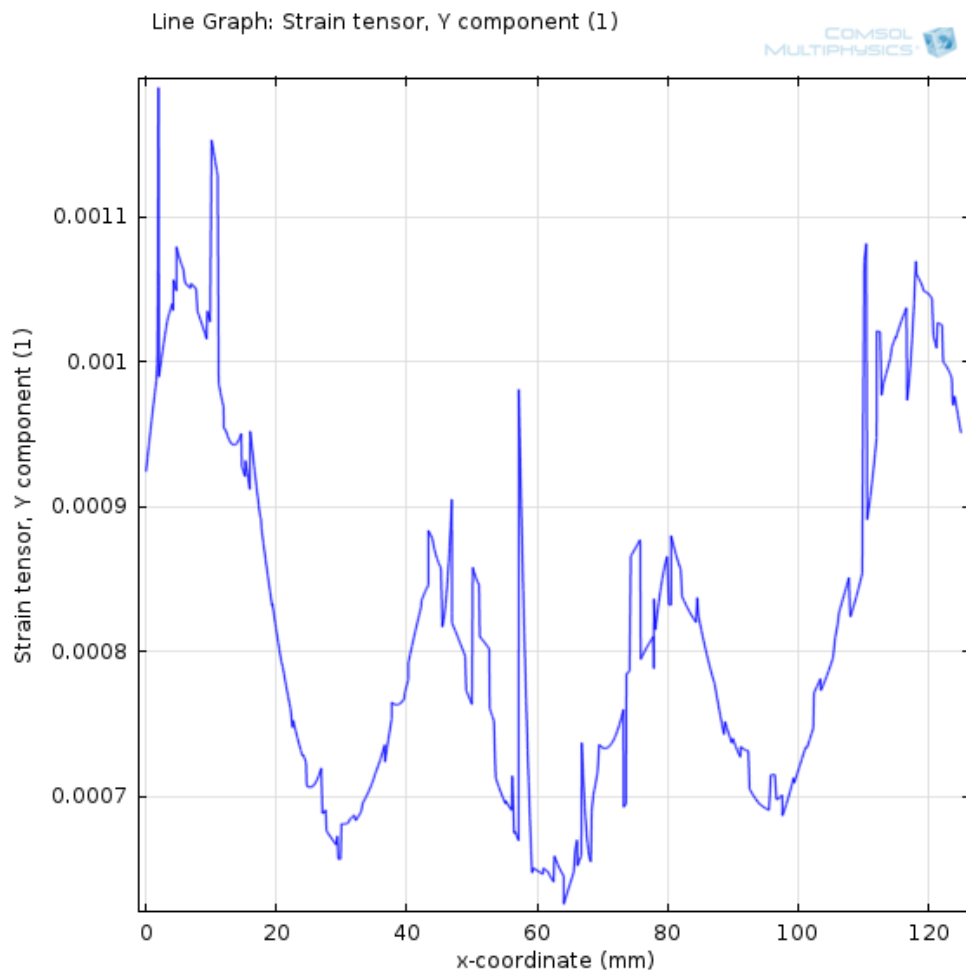


Figure 2.11: Simulation outcome of the y direction strain component across the A-A line.

## 2.4 Measurement description

This section gives a short description of the steps taken during measurement and introduces a few definitions that are used in describing the different states of the setup.

A function generator is used to produce a sine wave with desired frequency and amplitude, which is fed into a power supply current control input. In turn, the power supply generates the current, which is fed to the magnet. The amount of current through the wire feeding the magnet is measured using a zero flux meter. The data from the zero flux meter is saved during the measurement on the computer. Since a large NbTi AC superconducting dipole magnet with a well known field constant (33,3mT/A) is used, the corresponding field is readily determined.

For different values of field frequencies, the flux through the pickup- and compensation coil is measured. This is done for two distinct directions, which are referenced by the terms 'perpendicular' and 'parallel'. These naming corresponds to the direction of the field with respect to the the largest face of the stainless steel clamping plates. The values of the flux are recorded into the computer.

In the resulting data two different datasets are mentioned. One dataset is called 'empty coil' data, and references to a measurement with a certain magnetic field strength and frequency for which the pickup- and compensation coil signals are measured without a sample present in the setup. The other type of datasets is referenced to as 'sample data' or 'filled coil' data and indicates the presence of a sample during the acquisition of the displayed data. The empty coil data needs to be known since there may be loss sources that are not related to the sample (i.e. eddy currents in the clamping plates).

## 2.5 Data processing

This section explains how the data processing takes place. Since a completely new setup is used in this experiment, some data on magnetization is first acquired using an existing setup as a verification of the data.

The signals measured with the pickup and compensation coils are expected to be ahead in phase by 90 degrees from the magnetic field. To verify this, both the signals of the two coils as well as the zero flux signal from the power supply current lead are recorded. The zero flux signal is immediately translated in a magnetic field value by direct scaling. The raw data of such measurement is shown in figure 2.12.

From this data the magnetization of the sample can be determined. Matlab code was written to take care of all the steps. The mathematical process behind this calculation is elaborated in Appendix A. The calculated magnetization as a function of time for the data shown in figure 2.12 is given in figure 2.13. Before taking the summation, however, first the DC offset component of the signals is removed as the average over one period should be zero. If this step is omitted in processing the data, the resulting magnetization curves will not be closed loops.

By next subtracting the pickup coil and compensation coil integrated signals and plotting the result against the magnetic field, the magnetization curve results. The result for subtracting the empty coil signal from the pickup coil signal is shown in figure 2.14. Note that, in order to reveal more information about the characteristics of magnetization in figure 2.14 a linear regression between the compensation coil and pickup coil signal is used, such that the displayed result shows magnetization as  $M_{PU} - \alpha M_{CC}$  with  $\alpha$  the slope determined from the linear regression. Appendix B shows all calculated magnetization curves in a similar fashion.

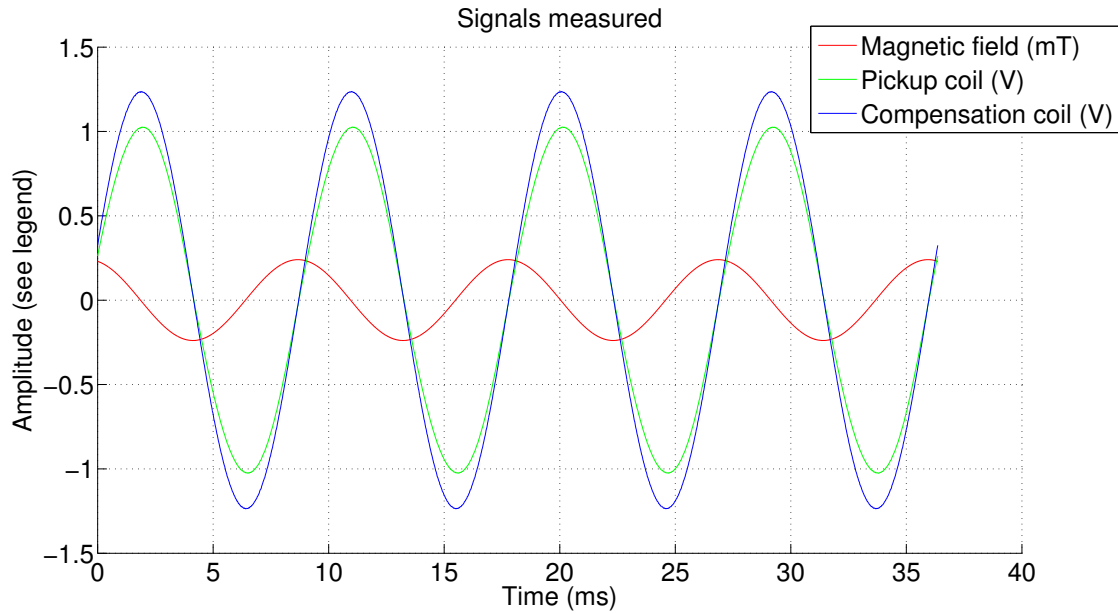


Figure 2.12: Field strength, pickup- and compensation coil measured signal from the measurement of the magnetization of the sample with a field oscillation amplitude  $B_a = 200\text{mT}$  and frequency  $f = 110\text{mHz}$

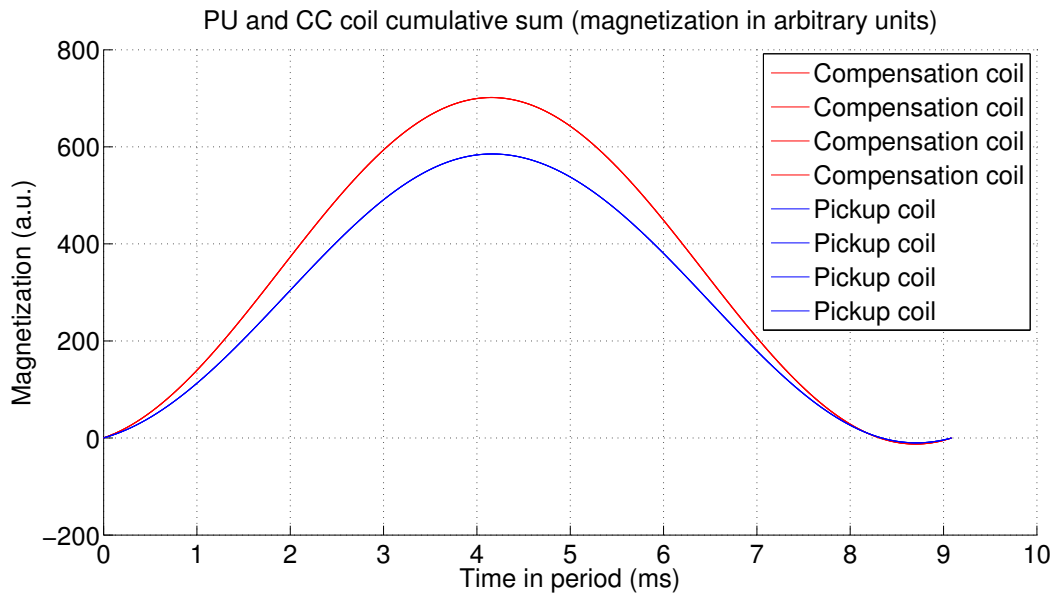


Figure 2.13: The cumulative sum of the pickup- and compensation coil signals for a field oscillation amplitude  $B_a = 200\text{mT}$  and frequency  $f = 110\text{mHz}$ . It can be clearly seen that the summation over one period is indeed zero.

Magnetization loops with sample,  $B = 200\text{mT}$ , perpendicular to clamp,  $P = 0\text{MPa}$ ,  $f = 110\text{mHz}$

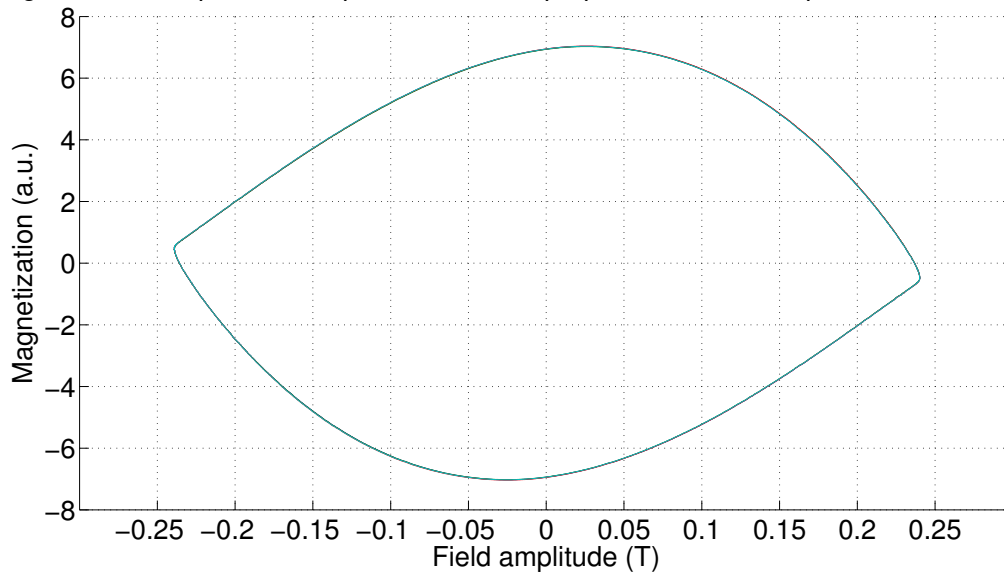


Figure 2.14: The magnetization curves of the difference between the pickup- and compensation coil for a field oscillation amplitude  $B_a = 200\text{mT}$  at a frequency of  $110\text{mHz}$ . The loops of four consecutive periods of the external field are shown.



# CHAPTER 3

## RESULTS

Following the routine described in section 1.2.3 the losses are determined from the pick-up and compensation coils under the the conditions prescribed in table 3.1.

100mT	Frequencies (mHz)	50, 150, 250, 350, 450
	Pressure on sample (MPa) @4.2K	0, 40, 80
	Orientation	parallel, perpendicular
200mT	Frequencies (mHz)	30, 50, 70, 90, 110
	Pressure on sample (MPa) @4.2K	0, 40, 80
	Orientation	parallel, perpendicular

Table 3.1: List of frequencies, pressures and orientations at which the sample is measured. The field strength is indicated by its amplitude.

As discussed in section 1.2.3, the frequency dependence of the loss per cycle  $Q_c$  allows to distinguish between the hysteresis and coupling loss. The data should follow a linear behaviour, with an intercept corresponding to the hysteresis loss and a slope indicative of the coupling loss. As explained in appendix A,  $Q_c$  is obtained by integrating the area enclosed by the magnetization loops  $M(H)$ . The loops themselves are shown in appendix B.

In this chapter only the frequency dependence of  $Q_c$  is shown, not the magnetization loops themselves. Figure 3.1 and 3.2 give the  $Q_c(f)$  data measured with the field perpendicular to the clamp, with an amplitude of 100mT and 200mT respectively. Note that all data are in arbitrary units, since exact calibration was not made, as explained in appendix B. However, relative comparison between losses measured under different conditions can still be made.

Comparing the hysteresis loss (intercept) between figure 3.1 and 3.2 we see how a doubling of the field amplitude leads to an increase of the loss with a factor  $\sim 10$ . This is consistent with the hysteresis loss measured in single tapes below the penetration field, where the loss is found to scale as  $Q_c(H) \propto H^3 \dots H^4$ , with  $H$  the applied field amplitude [6].

More puzzling is the increase of the hysteresis loss with applied pressure. According to the theory,  $Q_c$  should be proportional to the critical current and to the size of the tapes [3]. Since the size does not change significantly, the data seem to indicate that the critical current increases.

When next focussing on the coupling losses, i.e. the slope of the  $Q_c(f)$  curves, note that the data shown in figures 3.1, 3.2, 3.3 and 3.4 is corrected for empty coil effects. As discussed in section 2.4, the environment can also give rise to loss signals, which can be measured without the sample present and afterwards subtracted from the data with the sample present.

These empty coil measurements are also shown in figures B.1, B.5, B.9 and B.13 in appendix B. As seen in table 3.2, which summarizes the slopes and intercepts of all measurements, the empty coil signals also have a significant frequency dependence.

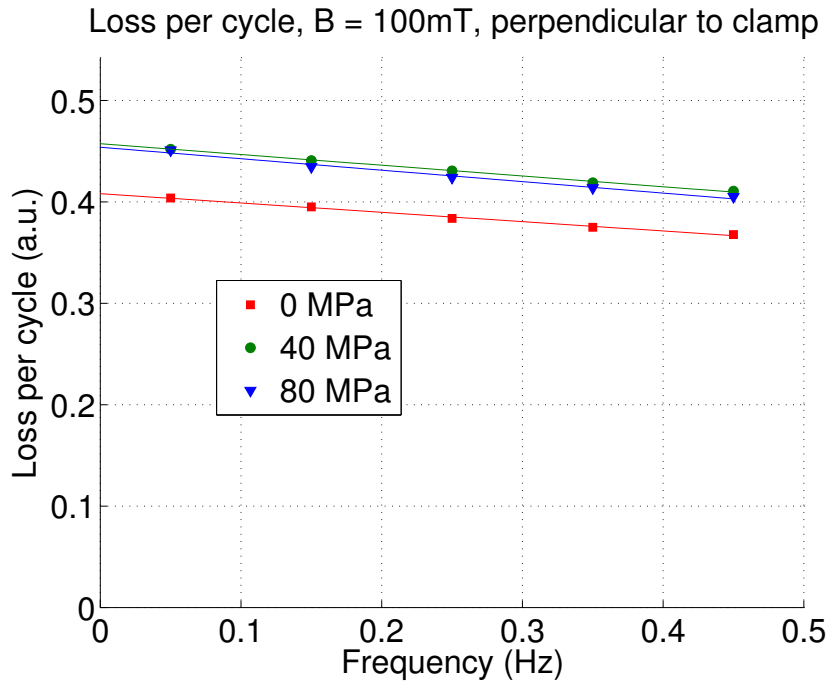


Figure 3.1: Losses per cycle for  $B_a = 100\text{mT}$ , perpendicular to the clamp plate. For the empty coil losses, refer to figure B.1.

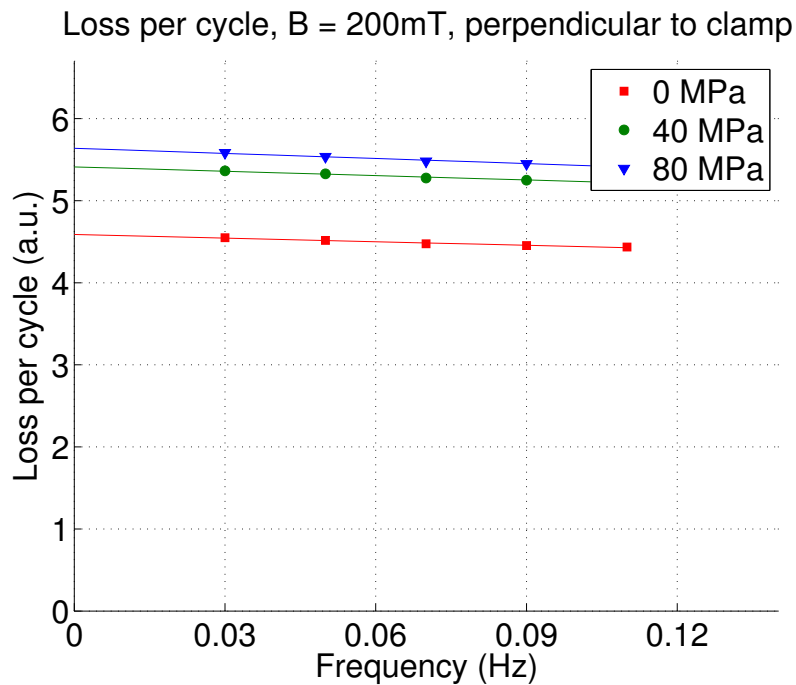


Figure 3.2: Losses per cycle for  $B_a = 200\text{mT}$ , perpendicular to the clamp plate. For the empty coil losses, refer to figure B.9.

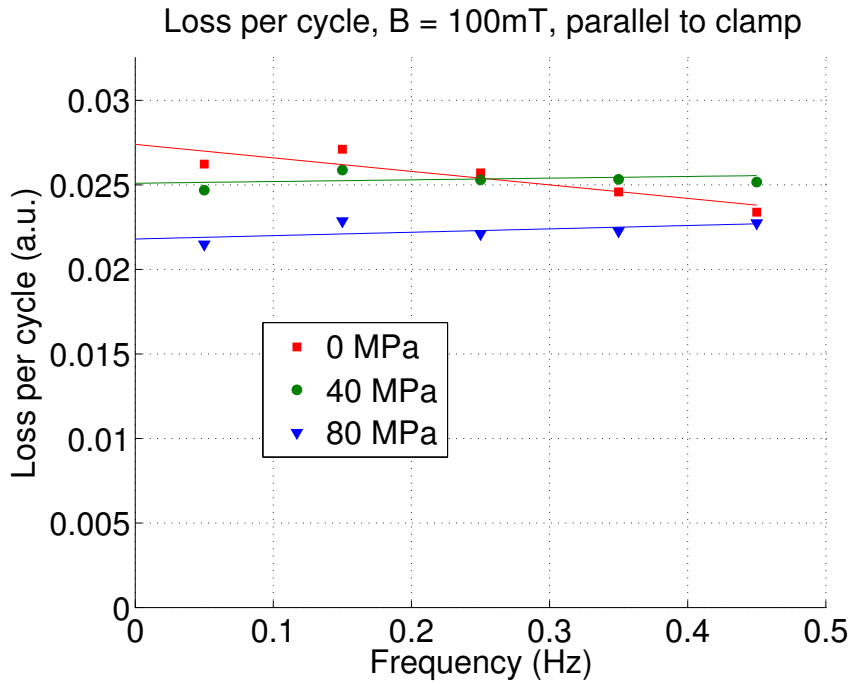


Figure 3.3: Losses per cycle for  $B_a = 100\text{mT}$ , parallel to the clamp plate. For the empty coil losses, refer to figure B.5.

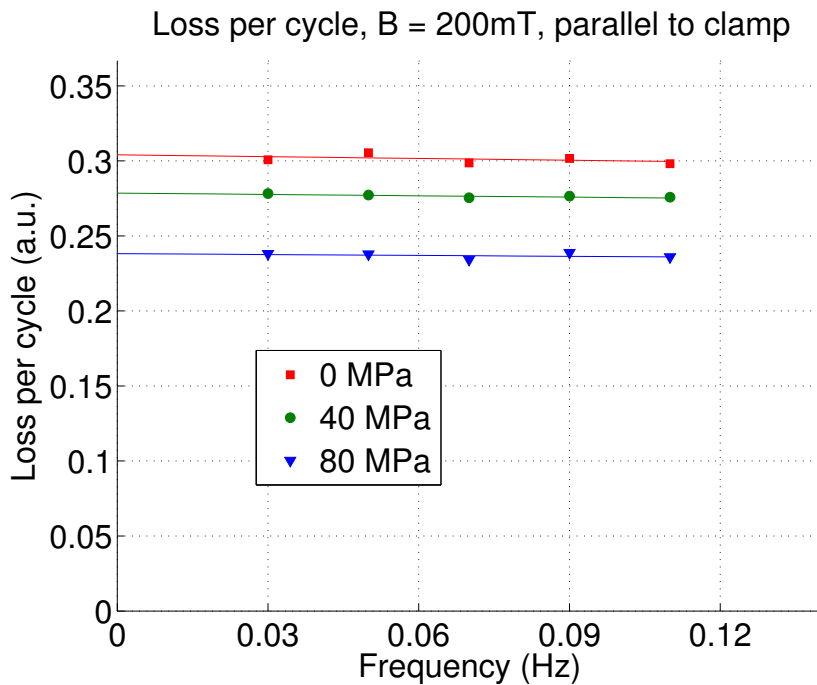


Figure 3.4: Losses per cycle for  $B_a = 200\text{mT}$ , parallel to the clamp plate. For the empty coil losses, refer to figure B.13.

Field amplitude (mT)	Orientation	Pressure (MPa)	Offset	Offset error	Slope	Slope error
100	parallel	empty coil	0.0041	0.0005	0.13	0.0019
		0	0.0315	0.0002	0.122	0.0008
		40	0.0292	0.0002	0.131	0.0006
		80	0.0259	0.0002	0.132	0.0007
200	parallel	empty coil	0.009	0.002	0.50	0.029
		0	0.313	0.002	0.46	0.020
		40	0.287	0.002	0.47	0.030
		80	0.247	0.002	0.48	0.031
100	perpendicular	empty coil	0.000	0.001	0.141	0.005
		0	0.409	0.002	0.049	0.007
		40	0.458	0.002	0.035	0.008
		80	0.454	0.004	0.028	0.013
200	perpendicular	empty coil	-0.008	0.005	0.57	0.067
		0	4.580	0.009	-0.90	0.123
		40	5.404	0.009	-1.20	0.124
		80	5.631	0.012	-1.50	0.156

Table 3.2: The intercepts (indicative for hysteresis loss) and the slopes (indicative for the coupling loss) of all measurements, including the error (95% confidence interval). Note the small difference in slope between the empty and filled coil data for the parallel orientation, indicating a significant contribution from the coil to the loss.

# CHAPTER 4

## DISCUSSION AND RECOMMENDATIONS

### 4.1 Phase shift in DC differential amplifiers

To come to a more readable result, the measured voltage from the pickup- and compensation coils are filtered using a 10Hz bandwidth filter with an amplification factor 20. When measuring AC losses, as pointed out in Appendix A, it is the phase difference between the applied field H and the subtraction of the two coil signals that determine the measure of AC loss. As the loss does not go linear with a phase shift in the measured signal, care must be taken to influence the phase as little as possible.

For the frequency range in this experiment, which is approximately a factor 100 below the cutoff frequency of the DC differential amplifiers, this should not be an issue for regular measurements. However, as the expected losses in this measurement are quite low, care should be taken to select an as high as possible bandwidth. In future experiments, the stability of the setup might be improved in terms of mechanical stability and field stability as well as noise reduction due to measuring at different setups in the lab at the same time. This enhancement in measurement environment might enable a higher bandwidth and therefore more accurate results

### 4.2 Power source dependence

In this experiment only limited field strength was available due to limitations in the power supply. A resulting consequence is the incomplete penetration of the field in the sample and therewith a reduction in measured coupling losses compared to maximum coupling losses.

It should therefore be taken into consideration to redo this experiment also at higher field strengths, or with non-zero offsets of the applied field.

### 4.3 Strain gauge values

There is a ambiguity on how to interpret the datasheet values on thermal contraction effects acting on the used strain gauges. This makes it difficult to verify the predicted actual stress on the sample. The uncertainty experienced in this experiment is mainly due to the uncertainty in the data on contraction. It is still unsure if the given data corresponds to a strain gauge suspended free in a medium or if some effects of a suspension are also recorded on the datasheet.

To reduce this uncertainty it would be recommend doing the experiment independently. That is, to measure the resistance of an unconstrained strain gauge at room temperature and next do the same at low temperatures of interest, liquid helium in this case. From this kind of measurement, more sensible conclusions can be drawn on the effects of thermal contraction on the used strain gauges.

## 4.4 Flow meter sensitivity and resolution

As the low  $\Delta P$  gas flow meter is a crucial step in the calibration and translation between arbitrary losses calculated with the use of the pickup- and compensation coil flux and the SI unit losses, a high resolution and stable flow signal are demanded for reproducible results.

During the measurement, an attempt is made to measure the flow with highest possible sensitivity. However, in an attempt to maximize sensitivity (and therewith resolution) at some point the gas flow started to oscillate in the system with flow meter saturation as a consequence.

The result of the oscillations made it that not the entire range of the flow meter is used. Whereas the maximum output value is 5 volt, the actual value used in this experiment was restricted to approximately 1 volt. As discussed in appendix B, this means that the loss data at present are effectively uncalibrated.

## 4.5 Changing amplification factors in the course of the experiment

It is important that the amplification factor of the DC differential amplifier does not change during the measurements, as well as in between two different measurement series. In case this value does change, for any reason, this may have a serious impact on the results. Although it is only a phase shift between the (integrated) coil signals and the current through the magnet that is of interest in determining the coupling losses, a change in amplitude might result in a relative change in signal.

During the learning curve of doing these experiments, the value of the amplifier was changed several times. Although good care is taken not to change it anymore from the point of starting the definitive measurements series, it is not 100% definite that this amplification factor did not change. It is of that reason, that it is suggested to redo the measurements again, noting the value of the amplification factor in the logbook as well, as this is not done during the measurements which form the base of this report.

## 4.6 Simulation of YBCO CORCC pressure dependence

Not as an improvement, but as a nice method of validating data and also to find in a less cost expensive way regions of interest as for what range of data points to measure, it will be useful to explore the options of simulating the actual experiment numerically. Some articles [7] about how to simulate YBCO already exist and described in deep detail how to describe flat YBCO cable behavior in magnetic fields. This information might form the base for the simulation of YBCO CORC cable layouts.

# APPENDIX A

## ANALYTICAL BACKGROUND OF THE DATA PROCESSING METHOD

The purpose of this appendix is to show the mathematical thoughts behind the steps in data processing as elaborated in section 2.5. This appendix involves a brief introduction to the used complex notation and continues with a mathematical step-by-step description of the measurement procedure and data processing steps.

### A.1 Complex numbers

When first coming across all analytical calculations involving complex numbers and functions, one might become confused simply by the different existing notations. It is for that reason that this section will elaborate on complex notation used in the following of this appendix.

From the Euler notation of complex numbers, it is known that

$$e^{i\phi} = \cos \phi + i \sin \phi. \quad (\text{A.1})$$

When working with pure sine wave signals, as is done in the case of this experiment for driving the current through the magnet, it may be convenient to rewrite the input wave form

$$V(t) = V_a \sin \omega t. \quad (\text{A.2})$$

In the complex notation, which using eulers formula in this situation gives

$$\tilde{V} = V_a e^{-i\frac{\pi}{2}} \quad (\text{A.3})$$

The transformation from the complex domain to the real domain is rather straight forward. The transformation is giving by multiplying the complex function with  $e^{i\omega t}$  and taking the real part of the resulting number, so in the case currently at hand

$$V(t) = \text{Re}[\tilde{V} e^{i\omega t}] = \text{Re}[\tilde{V} (\cos \omega t + i \sin \omega t)]. \quad (\text{A.4})$$

When taking the time derivative of a complex function as used above, writing the complex function to its real valued counterpart, differentiating the function and writing it back in its complex notation learns that

$$\frac{d\tilde{A}}{dt} = i\omega\tilde{A}. \quad (\text{A.5})$$

### A.2 Magnetic field

The sine wave voltage signal generated with a function generator is used to drive the power supply that feeds the magnet. In complex notation the output of the function generator is described as

$$f(t) = V_a \sin \omega t \Rightarrow \tilde{f}(t) = V_a e^{-i\frac{\pi}{2}}. \quad (\text{A.6})$$

With the gain of the power source given by  $\alpha$  and the magnet constant is given by  $\beta$ , the magnetic field is given by

$$\tilde{H} = H_0 e^{-i\frac{\pi}{2}} = -iH_0 \quad (\text{A.7})$$

where  $H_0$  absorbs all constant terms ( $\mu_0, \alpha, \beta$ ).

### A.3 Coil signals

The definition of magnetic flux is given by the surface integral over a closed area  $S$  by

$$\Phi = \oint \mathbf{B} \cdot d\mathbf{a}. \quad (\text{A.8})$$

The resulting electromotive force (e.m.f,  $\mathcal{E}$ ) due to a flux change is given by

$$\mathcal{E} = -\frac{d\Phi}{dt} \quad (\text{A.9})$$

and the magnetic field  $\mathbf{B}$  is given by

$$\mathbf{B} = \mu_0(\mathbf{H} + \mathbf{M}), \quad (\text{A.10})$$

where  $\mathbf{M}$  represents the magnetization of an object enclosed by the surface  $S$ . The expected e.m.f. can then be calculated. Dropping the vector notation for  $\mathbf{B}$ ,  $\mathbf{H}$  and  $\mathbf{M}$  as they will in our case always be parallel or perpendicular with respect to each other, it then follows that the e.m.f. is given by

$$\tilde{\mathcal{E}} = -c_0 \left( \frac{d\tilde{H}}{dt} + \frac{d\tilde{M}}{dt} \right) = c_0 i\omega (\tilde{H} + \tilde{M}) \quad (\text{A.11})$$

where  $c_0$  absorbs all constant terms again ( $H_0, \mu_0$ ). Now there are two separate cases to consider. In the case of the compensation coil, the magnetization should be  $\tilde{M} = 0$  as there should not be anything near the compensation coil that could be magnetized. On the other hand, the pickup coil encloses or is close to a source of sample magnetization and thus the pickup coil term  $\tilde{\mathcal{E}}_{PU}$  should carry the effect of the magnetization term.

For the voltmeter connected to the compensation coil, the sensed signal is the real part of  $\tilde{\mathcal{E}}_{CC}$  which equals

$$\mathcal{E}_{CC} = \text{Re} \left[ \tilde{\mathcal{E}}_{CC} e^{i\omega t} \right] = -c_0 \omega \cos \omega t \quad (\text{A.12})$$

which means that the amplitude of the signal measured by the compensation coil should be proportional to the frequency. Verification of this on the measurement data shows this is indeed the case.

The signal of the pickup coil sensed by the voltmeter is a little more complicated due to the complex magnetization term that is now included. The complex magnetization can be written as

$$\tilde{M} = \tilde{\chi}_m \tilde{H} \quad (\text{A.13})$$

so that the complex flux through the pickup coil can be written as

$$\tilde{\mathcal{E}}_{PU} = -c_0 \left( \frac{d\tilde{H}}{dt} + \frac{d[\tilde{\chi}_m \tilde{H}]}{dt} \right). \quad (\text{A.14})$$

Taking into account the special rule for time derivatives of complex functions mentioned in section A.1 and applying the product rule for derivatives the same way as for real valued functions it then follows that

$$\tilde{\mathcal{E}}_{PU} = -i\omega c_0 \tilde{H} (1 + 2\tilde{\chi}_m) \quad (\text{A.15})$$

In the real domain the signal sensed by the voltmeter is than

$$\mathcal{E}_{PU} = \text{Re} \left[ \tilde{\mathcal{E}}_{PU} e^{i\omega t} \right] = -c_0 \omega (\cos \omega t + 2\chi_m \cos(\omega t + \phi_\chi)) \quad (\text{A.16})$$

Now in the ideal case the subtracted signal

$$\Delta \mathcal{E} \equiv \mathcal{E}_{PU} - \mathcal{E}_{CC} \quad (\text{A.17})$$

gives the following interesting result

$$\Delta \mathcal{E} = -2c_0 \omega \chi_m \cos(\omega t + \phi_\chi), \quad (\text{A.18})$$

which means that the difference of the two coil signals is purely non-zero because of a phase component  $\phi_\chi$  that results from the magnetization of the object inside or nearby the pickup coil. Note that this phase is relative to the phase of the current generating the magnetic field. Also notice that what is actually calculated (or measured) here is the time derivative of the magnetization of the sample, that is

$$\Delta \mathcal{E} \propto -\frac{dM}{dt}. \quad (\text{A.19})$$

## A.4 Higher harmonics of the magnetization

One downside of the derivation given above is that the use of complex notation throws away all information about higher harmonics of the magnetization signal (as you explicitly assume a frequency  $\omega$  when transforming between the real and complex notation). Although these terms do actually exist in the real world, also during the measurements described in this report, they are of no physical interest when calculating AC losses.

To understand this, the magnetization of an object may be written as a Fourier series. Doing this, the real valued magnetization looks like

$$M = a_0 + \sum_{n=1}^{\infty} [a_n \cos(n\omega_0 t) + b_n \sin(n\omega_0 t)]. \quad (\text{A.20})$$

As the AC loss is calculated using the following property from statistical physics [3]

$$Q_c = \frac{1}{\mu_0} \oint M dH = \frac{1}{\mu_0} \int_{t=0}^T M \frac{dH}{dt} dt, \quad (\text{A.21})$$

and as the field  $H$  in the case of this experiment is (considered to be) a pure sine wave, it follows that only the first order term  $a_1 \cos(\omega_0 t)$  will integrate to a non-zero value over an entire period (applying the nature of the orthogonality of sine- and cosine waves).

In other words, only the component of the magnetization at the fundamental frequency, but shifted  $90^\circ$  in phase with respect to  $H$ , gives rise to hysteresis loss.



## APPENDIX B

# CALCULATED MAGNETIZATION CURVES AND LOSS PLOTS

This appendix shows all magnetization curves of both the empty coil and filled coil measurements. To show the superconducting nature of the sample, the values found for the magnetization of the pickup and compensation coil signals are modified in such a way (using a linear regression) that the displayed result of all magnetizations in this section is given by

$$M = M_{PU} - \alpha M_{CC} \quad (\text{B.1})$$

with  $\alpha$  the slope between  $M_{CC}$  and  $M_{PU}$  found with a linear regression. The values of the loss per cycle shown in this appendix are the result of integrating the areas of the shown magnetization curves. Note that the outcome of the integration does not depend on the regression correction used to display the curves.

All next figures form sets of four, that is, the first out of four figures shows the empty coil data and the next three figures show the data for the different applied pressures (0MPa, 40MPa and 80MPa). To see the resulting sample loss per cycle, please refer to figures 3.1, 3.2, 3.3 and 3.4 in the results chapter of this report (chapter 3). For the errors in the  $Q_c(f)$  plots given in this appendix, the reader is referred to table 3.2.

Note that all magnetization  $M(H)$  and loss per cycle  $Q_c(f)$  data are given in arbitrary units. As already indicated in 2.2, the calibration of inductive loss measurements is a delicate process, involving the geometry and relative position of the pickup coils and the sample.

The usual trick used with this set-up, to calibrate the inductive data with the calorimetric data, could not be applied for these measurements, since the losses in these relatively small samples<sup>1</sup> were too low to get a clear calorimetric signal.

Therefore, in this report the data is presented 'as is', in terms of integrated voltages. Note that relative information can still be obtained from, since the calibration factors do not depend on frequency, amplitude or pressure on the sample. Direct comparison between the magnitude of the perpendicular and parallel signals, however, is not possible since they are measured with different coil sets.

---

<sup>1</sup>The used set-up is designed to study low-temperature superconducting cable samples, with typically  $\sim 10 - 100$  times larger volume than the measured CORC cable sample in this experiment.

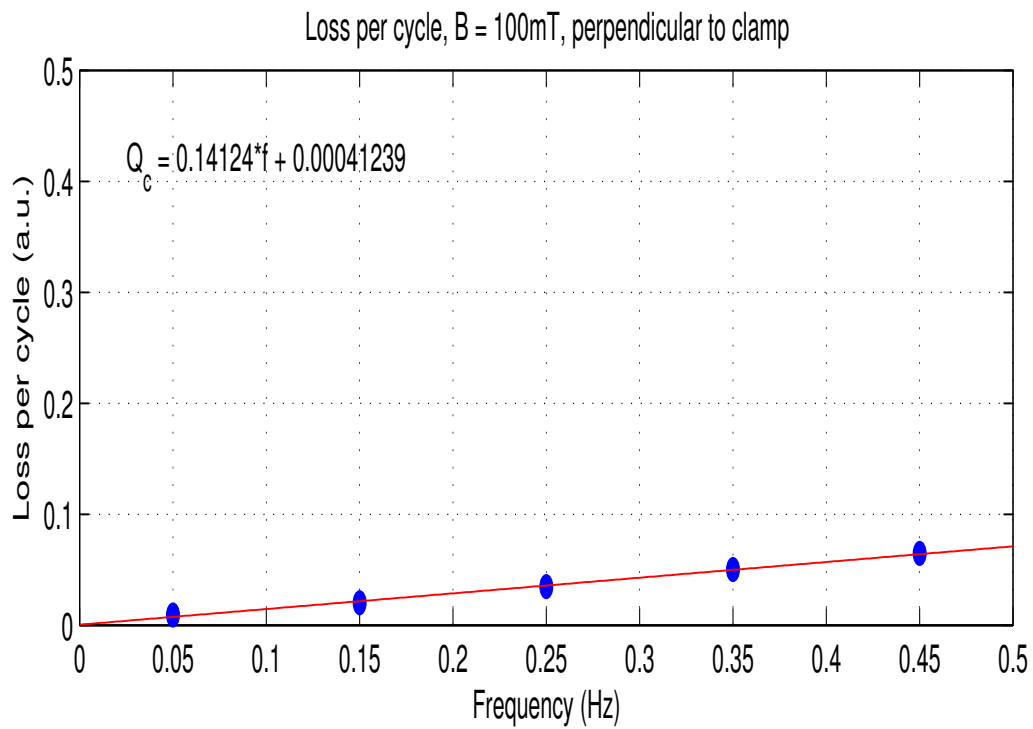
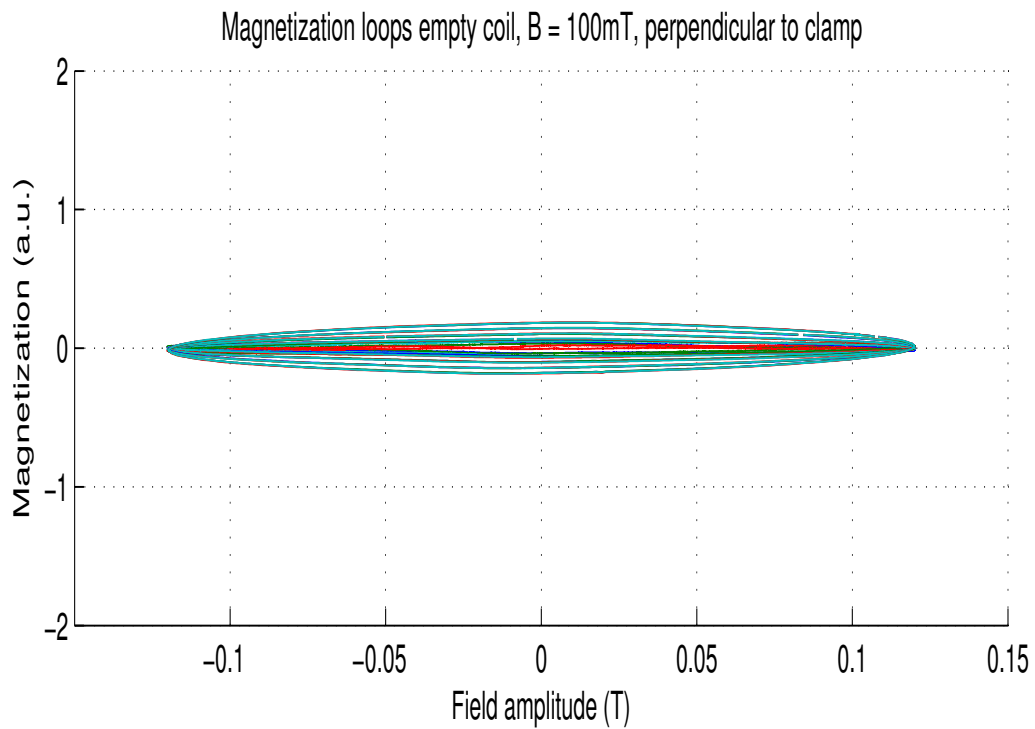


Figure B.1: *Top*:  $M(H)$  loops for each frequency (inner loop corresponding with the lowest frequency) and *Bottom*: loss per cycle  $Q_c(f)$  measured without the sample in a 100mT field, perpendicular to the clamp.

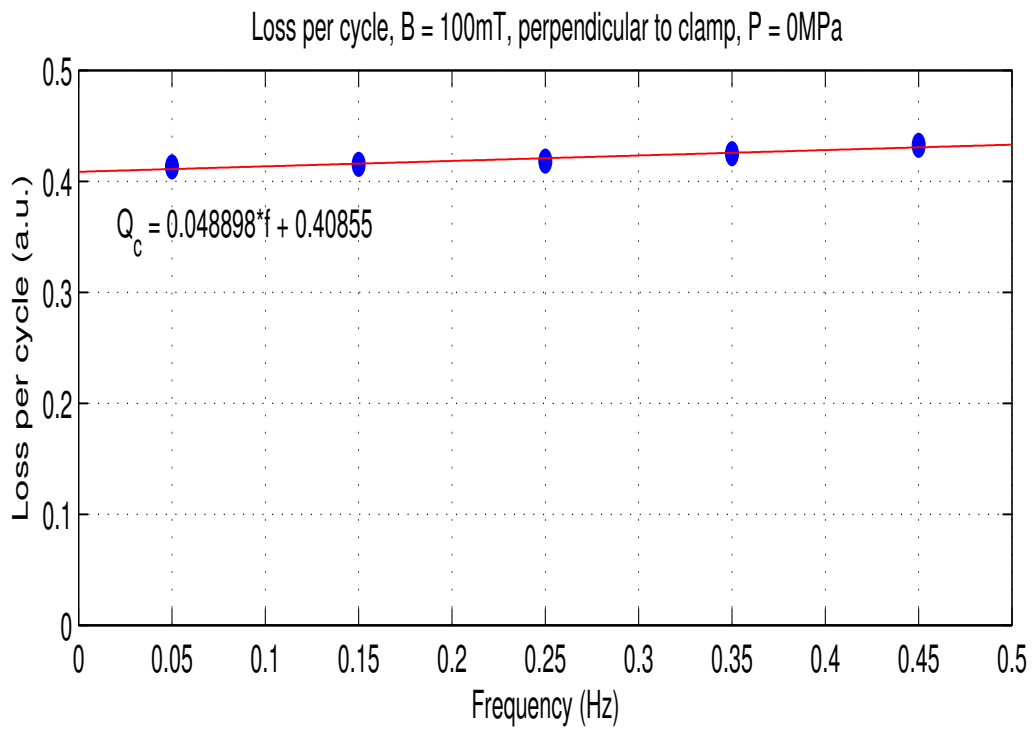
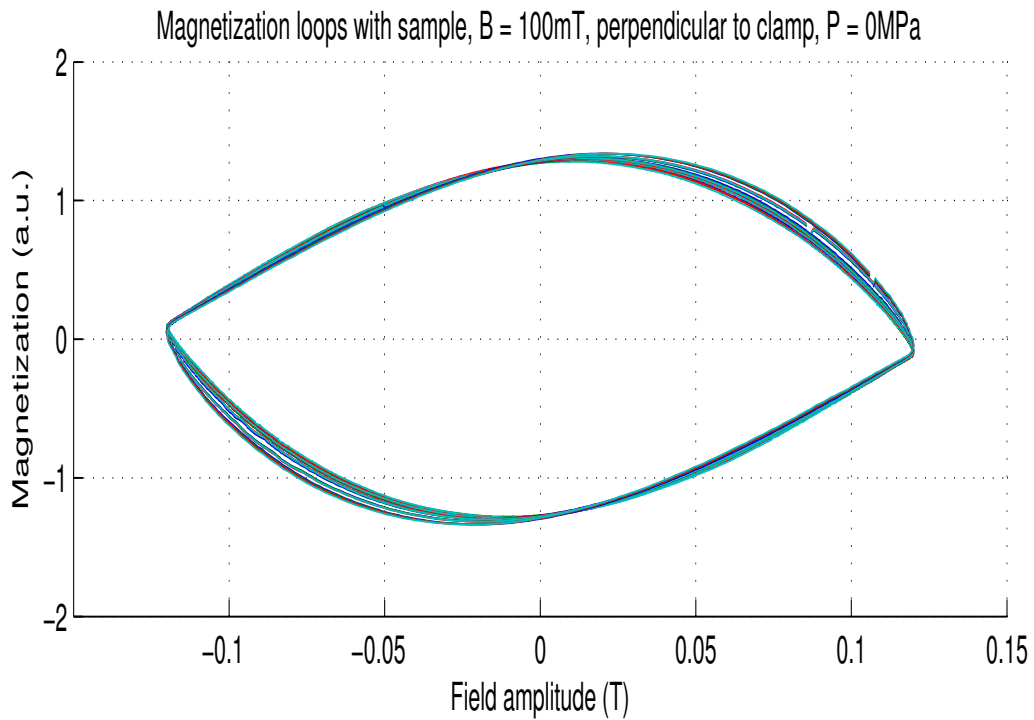


Figure B.2: *Top*: M(H) loops for each frequency (inner loop corresponding with the lowest frequency) and *Bottom*: loss per cycle  $Q_c(f)$  measured with the sample in a 100mT field, perpendicular to the clamp and no pressure.

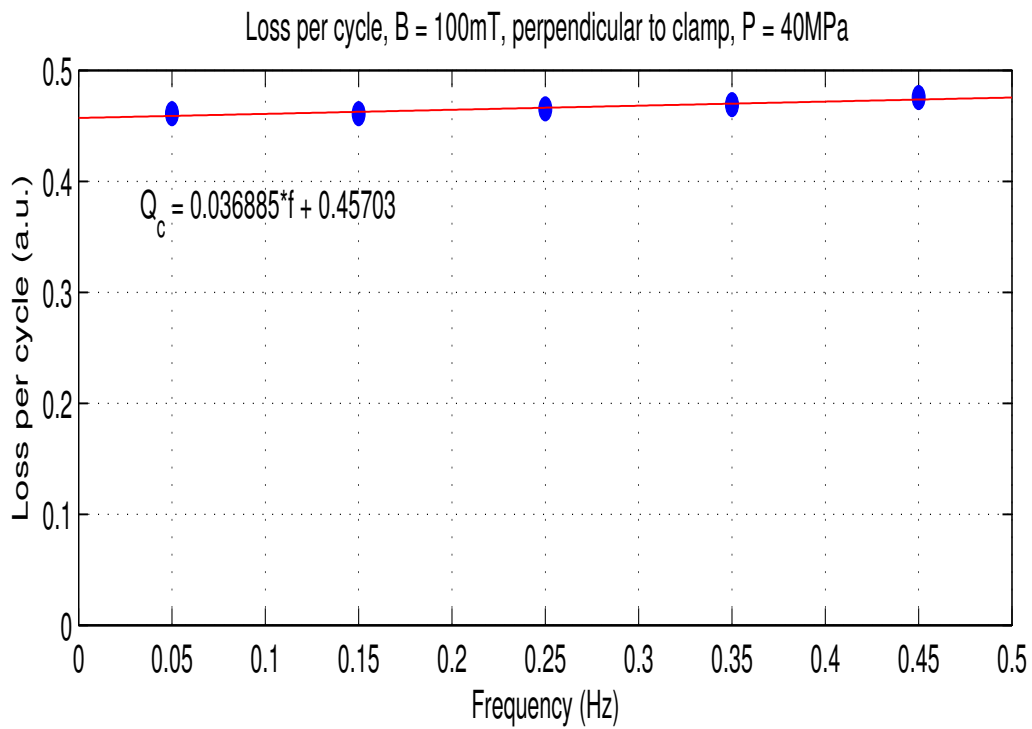
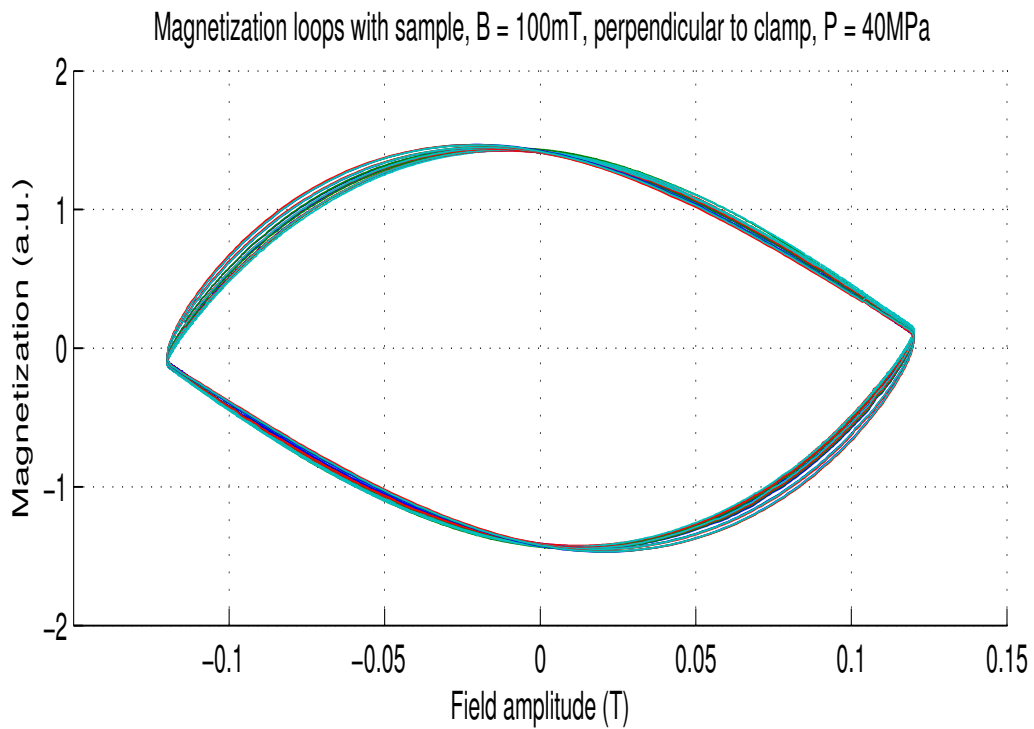


Figure B.3: *Top*: M(H) loops for each frequency (inner loop corresponding with the lowest frequency) and *Bottom*: loss per cycle  $Q_c(f)$  measured with the sample in a 100mT field, perpendicular to the clamp and 40MPa pressure.

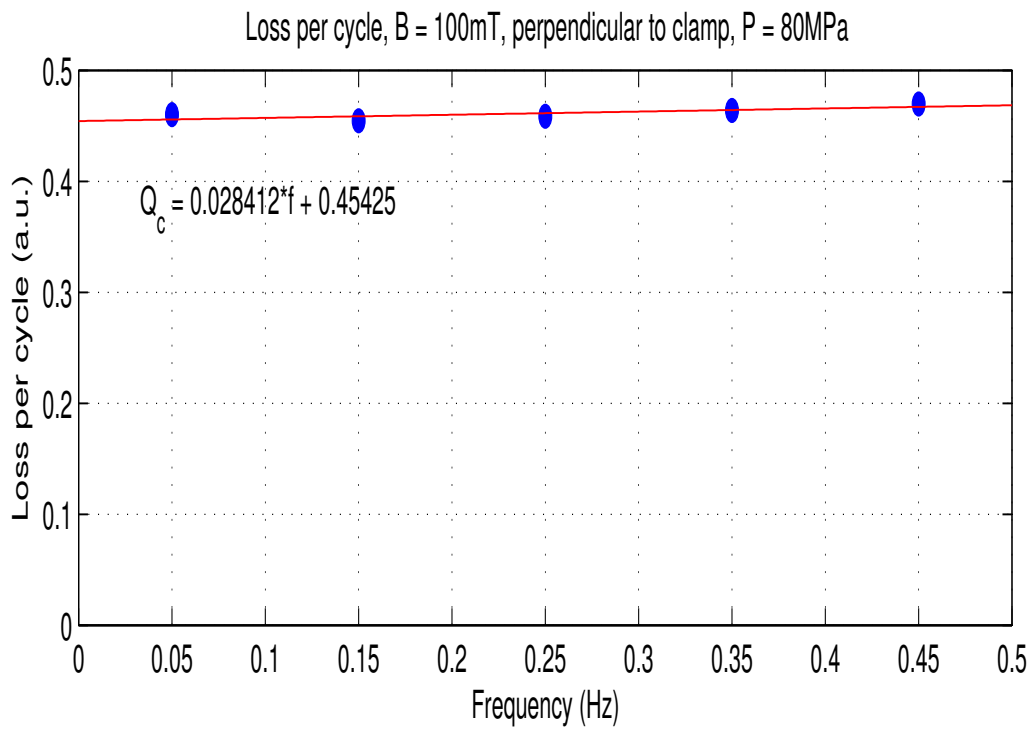
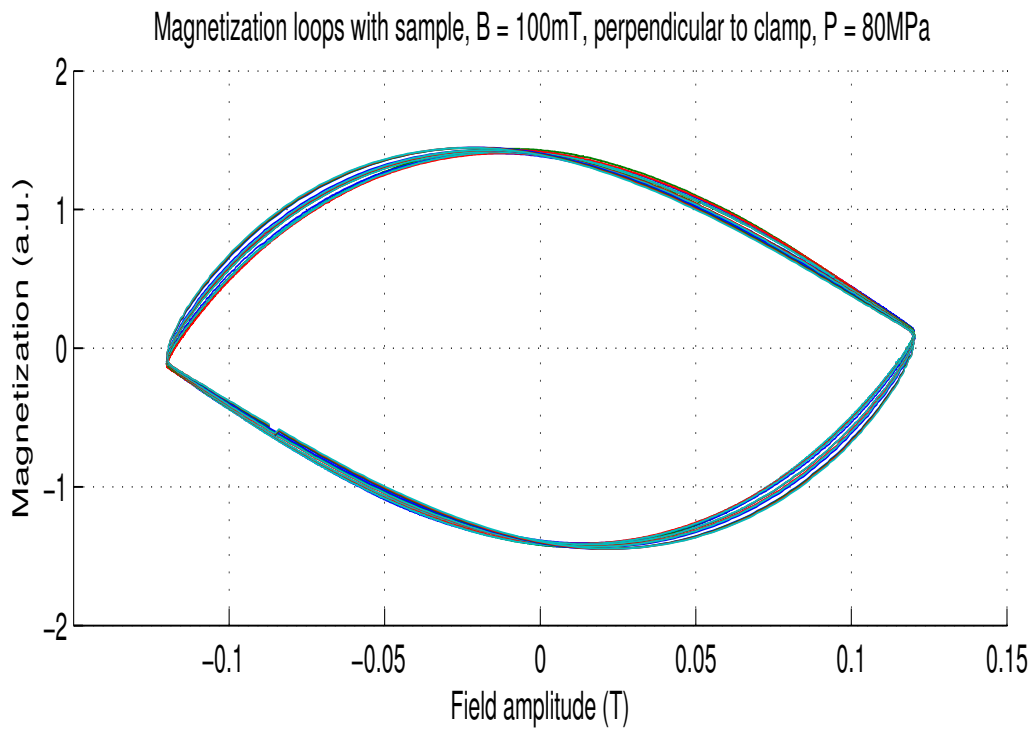


Figure B.4: *Top*: M(H) loops for each frequency (inner loop corresponding with the lowest frequency) and *Bottom*: loss per cycle  $Q_c(f)$  measured with the sample in a 100mT field, perpendicular to the clamp and 80MPa pressure.

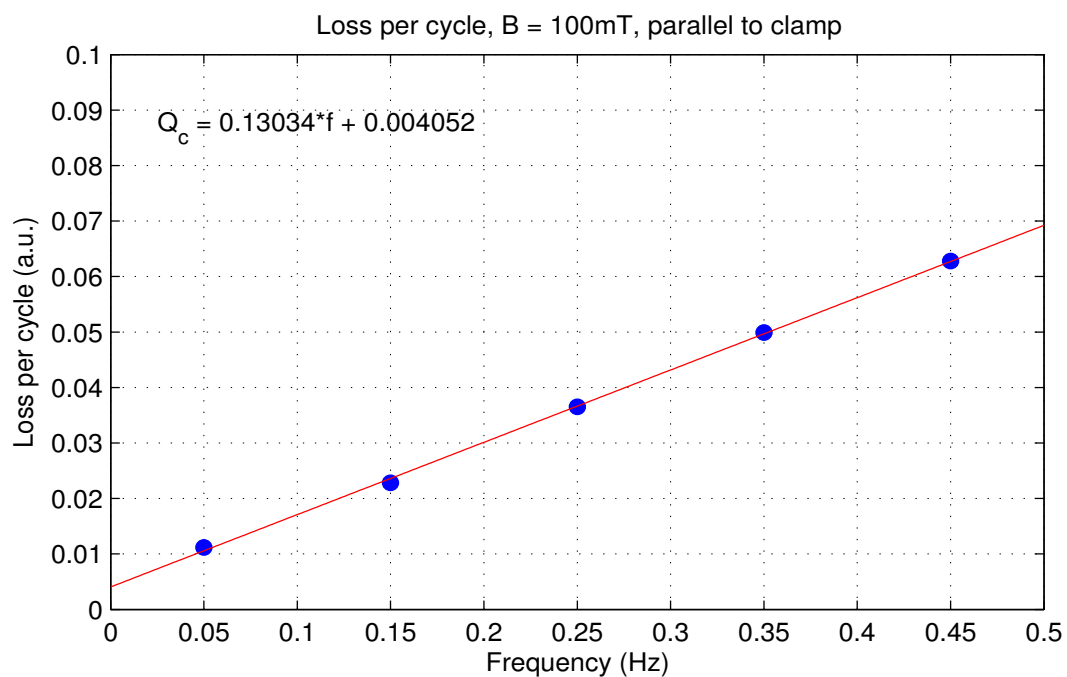
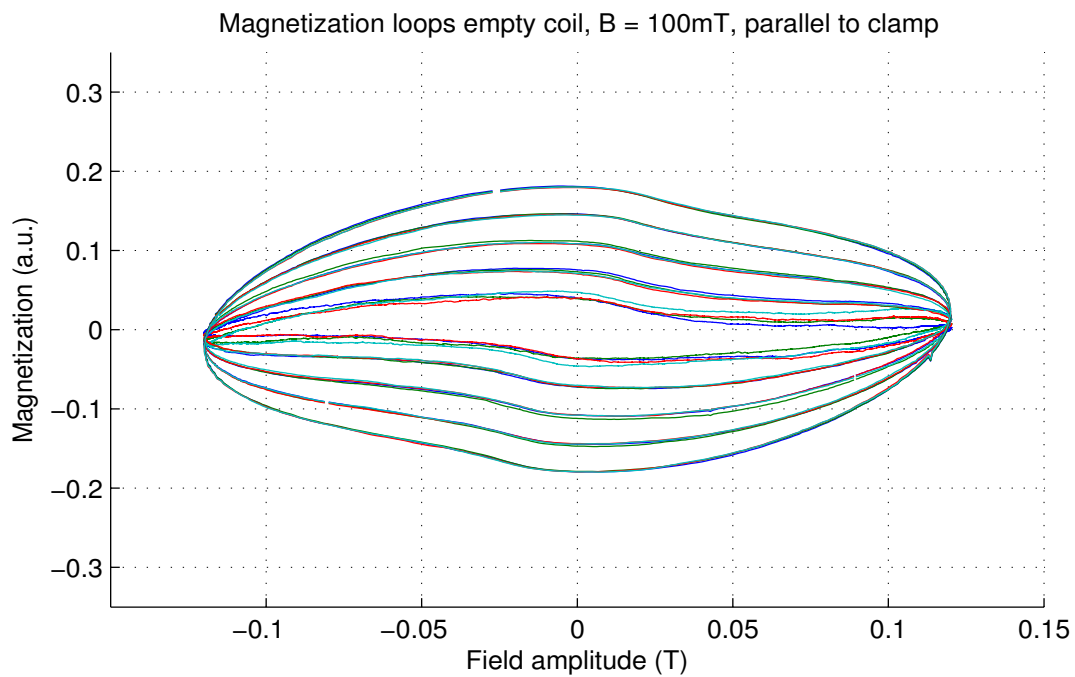


Figure B.5: *Top*:  $M(H)$  loops for each frequency (inner loop corresponding with the lowest frequency) and *Bottom*: loss per cycle  $Q_c(f)$  measured without the sample in a 100mT field, parallel to the clamp.

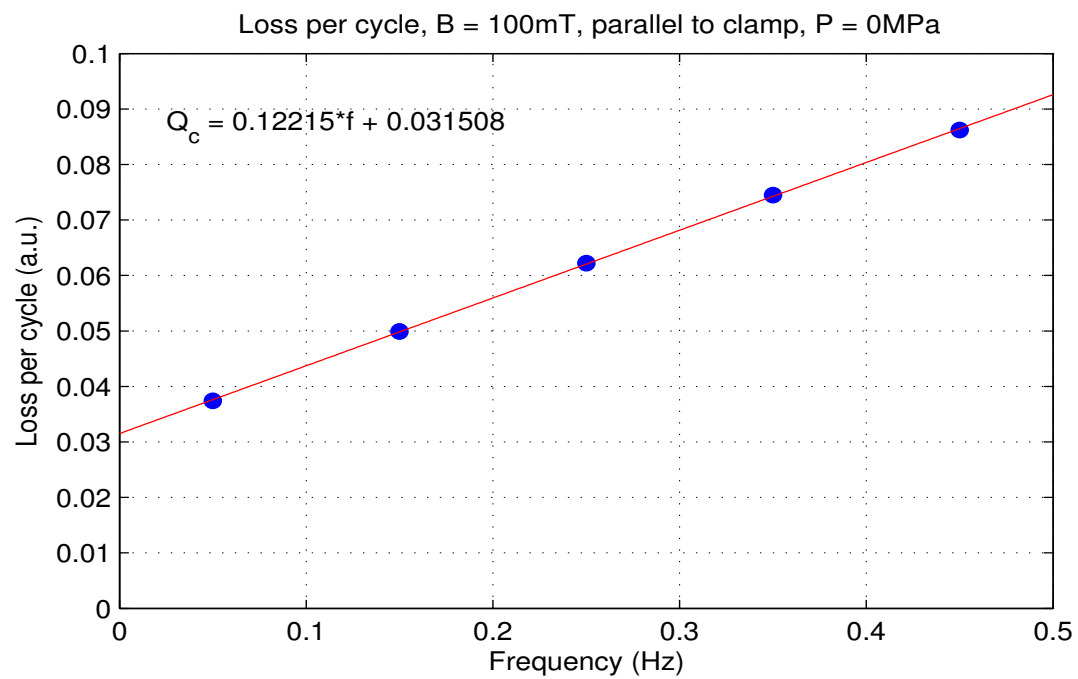
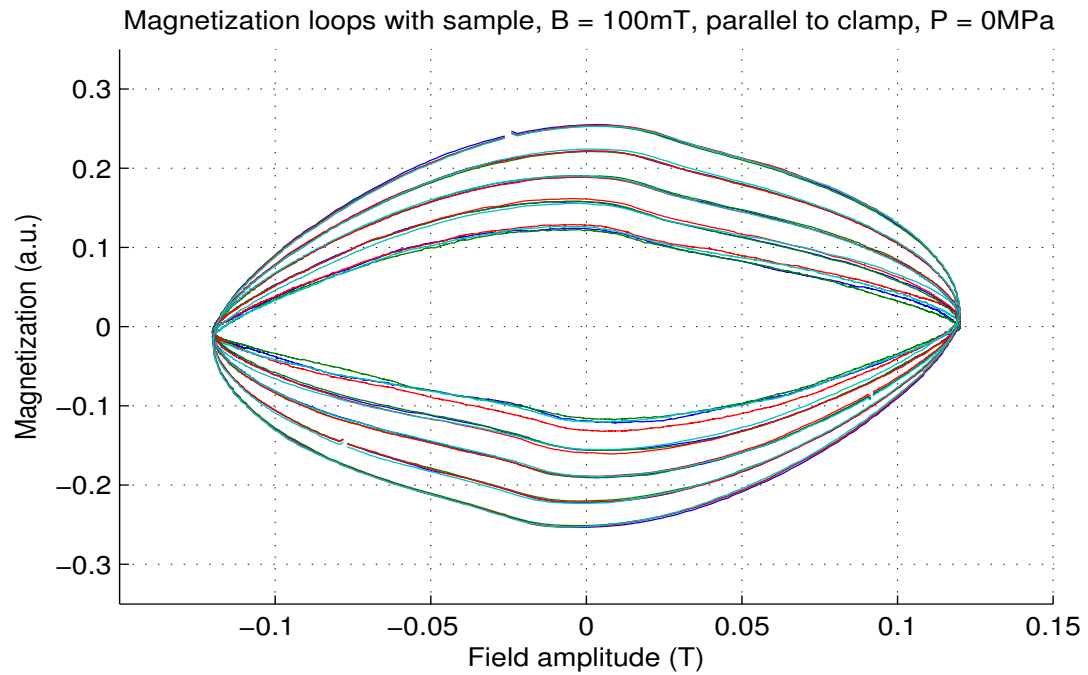


Figure B.6: *Top*:  $M(H)$  loops for each frequency (inner loop corresponding with the lowest frequency) and *Bottom*: loss per cycle  $Q_c(f)$  measured with the sample in a 100mT field, parallel to the clamp and no pressure.

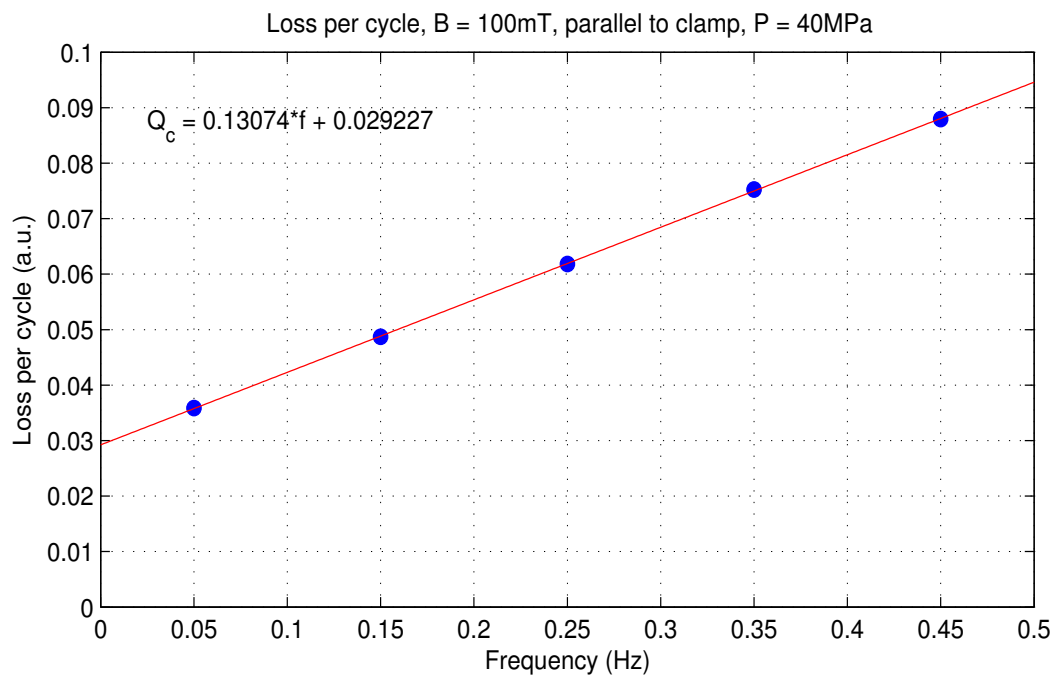
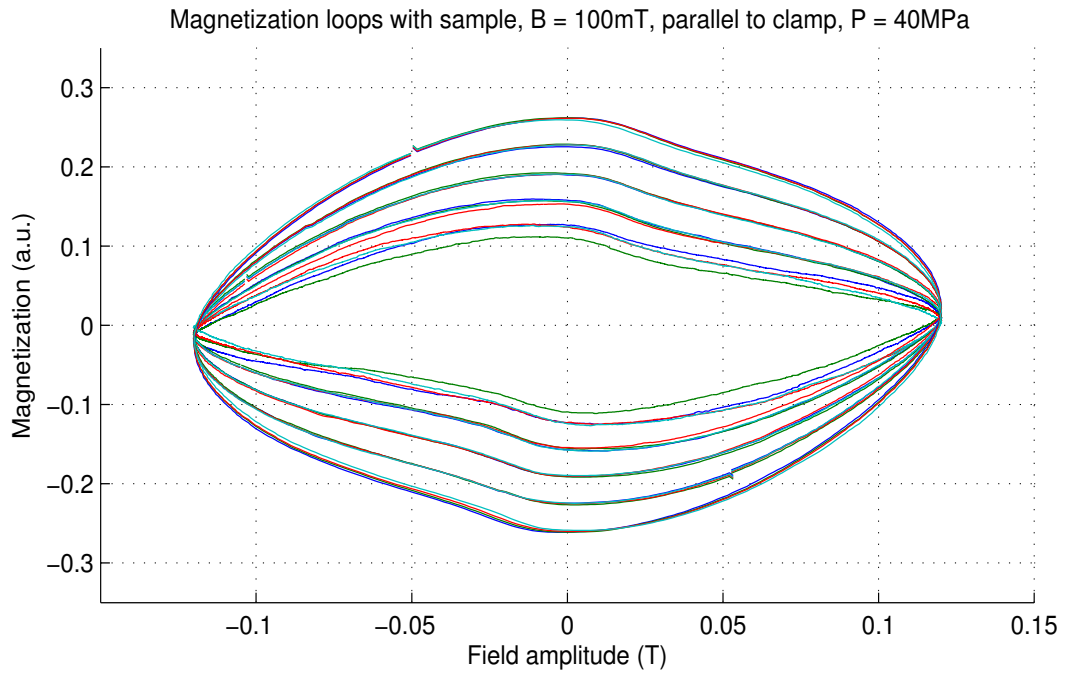


Figure B.7: *Top*:  $M(H)$  loops for each frequency (inner loop corresponding with the lowest frequency) and *Bottom*: loss per cycle  $Q_c(f)$  measured with the sample in a 100mT field, parallel to the clamp and 40MPa pressure.

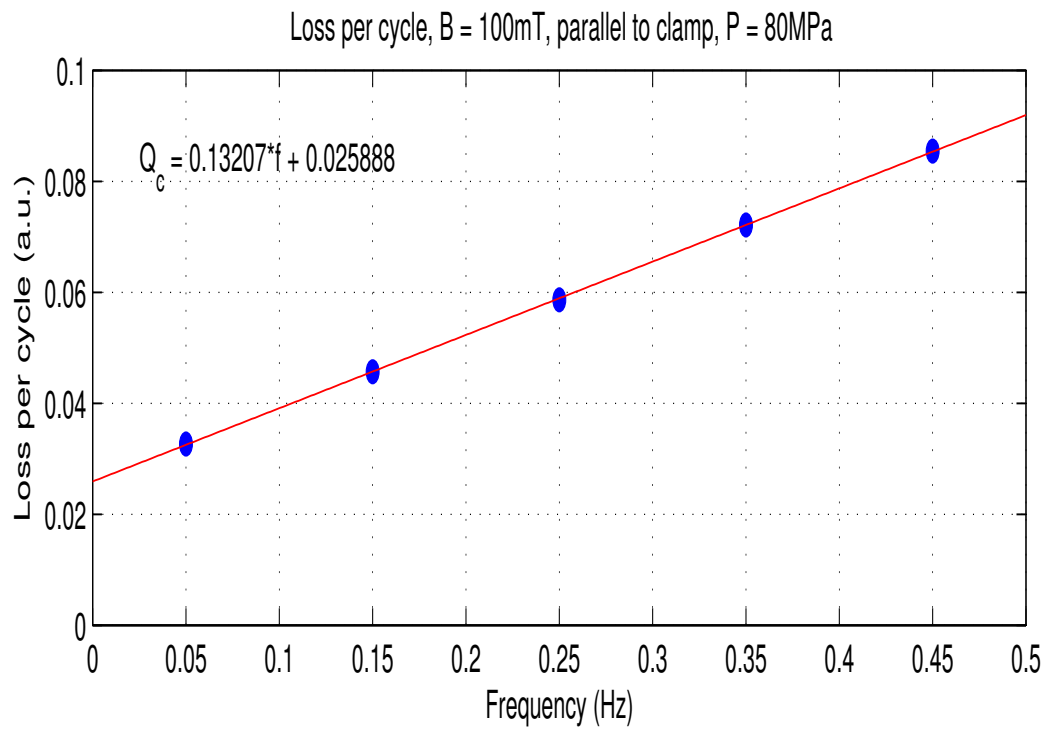
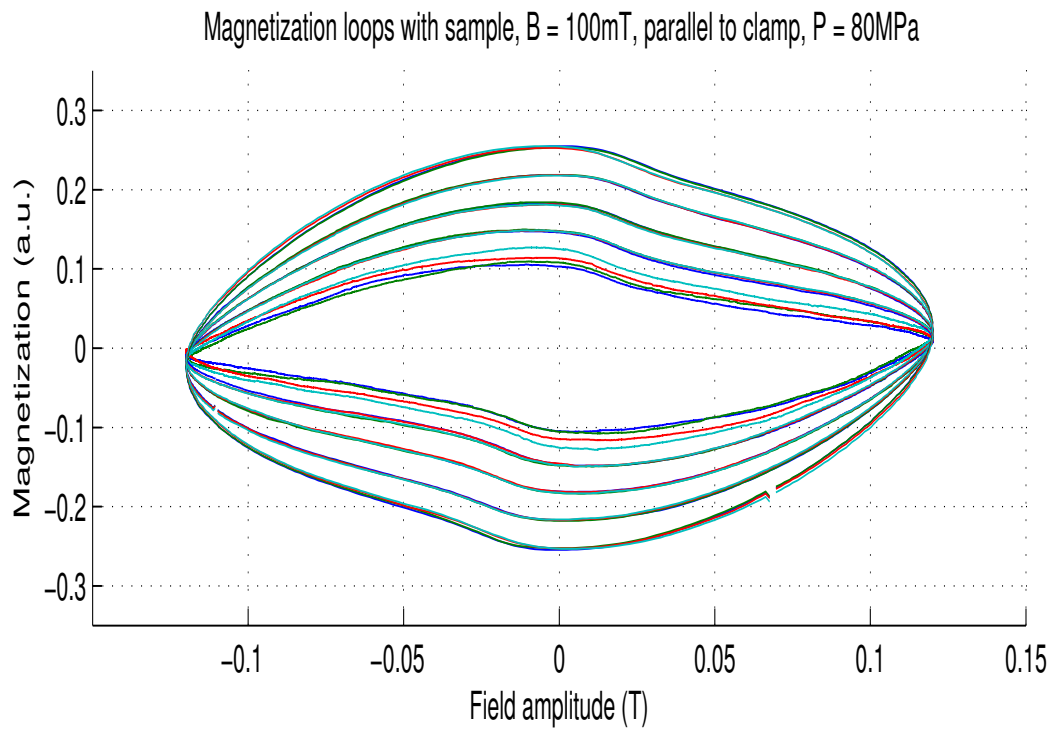


Figure B.8: *Top*:  $M(H)$  loops for each frequency (inner loop corresponding with the lowest frequency) and *Bottom*: loss per cycle  $Q_c(f)$  measured with the sample in a 100mT field, parallel to the clamp and 80MPa pressure.

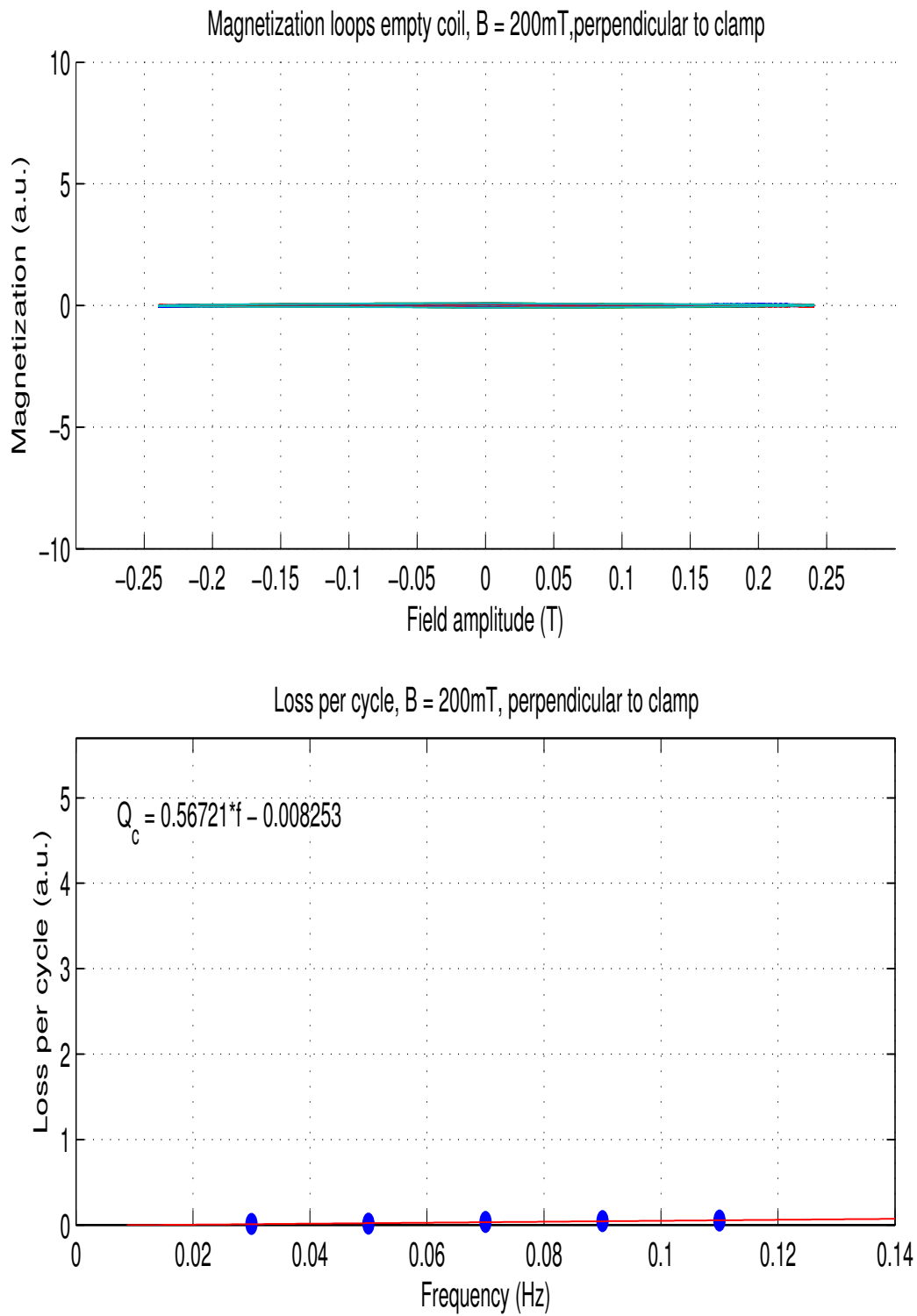


Figure B.9: *Top*: M(H) loops for each frequency (inner loop corresponding with the lowest frequency) and *Bottom*: loss per cycle  $Q_c(f)$  measured without the sample in a 200mT field, perpendicular to the clamp.

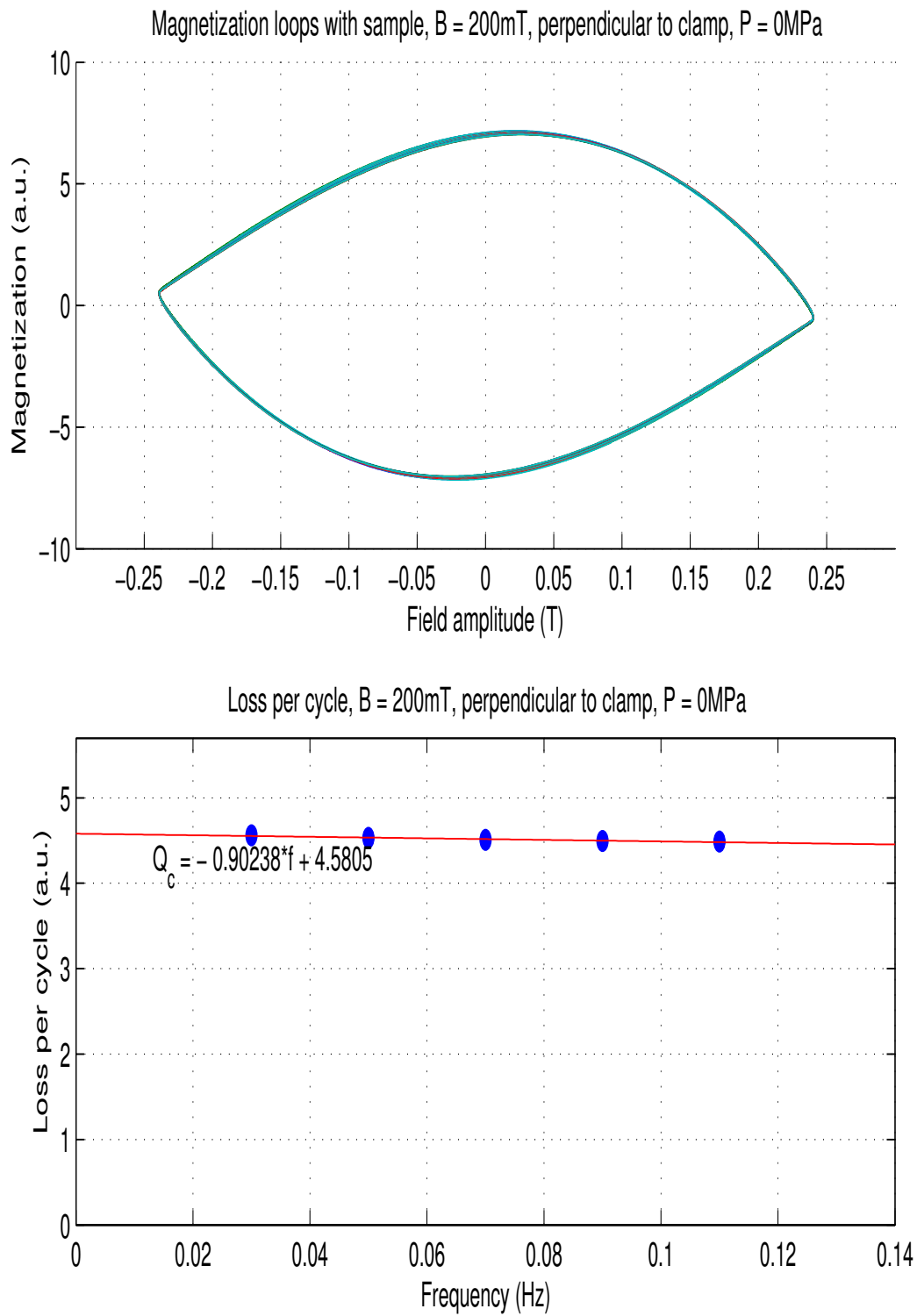


Figure B.10: *Top*: M(H) loops for each frequency (inner loop corresponding with the lowest frequency) and *Bottom*: loss per cycle  $Q_c(f)$  measured with the sample in a 200mT field, perpendicular to the clamp and no pressure.

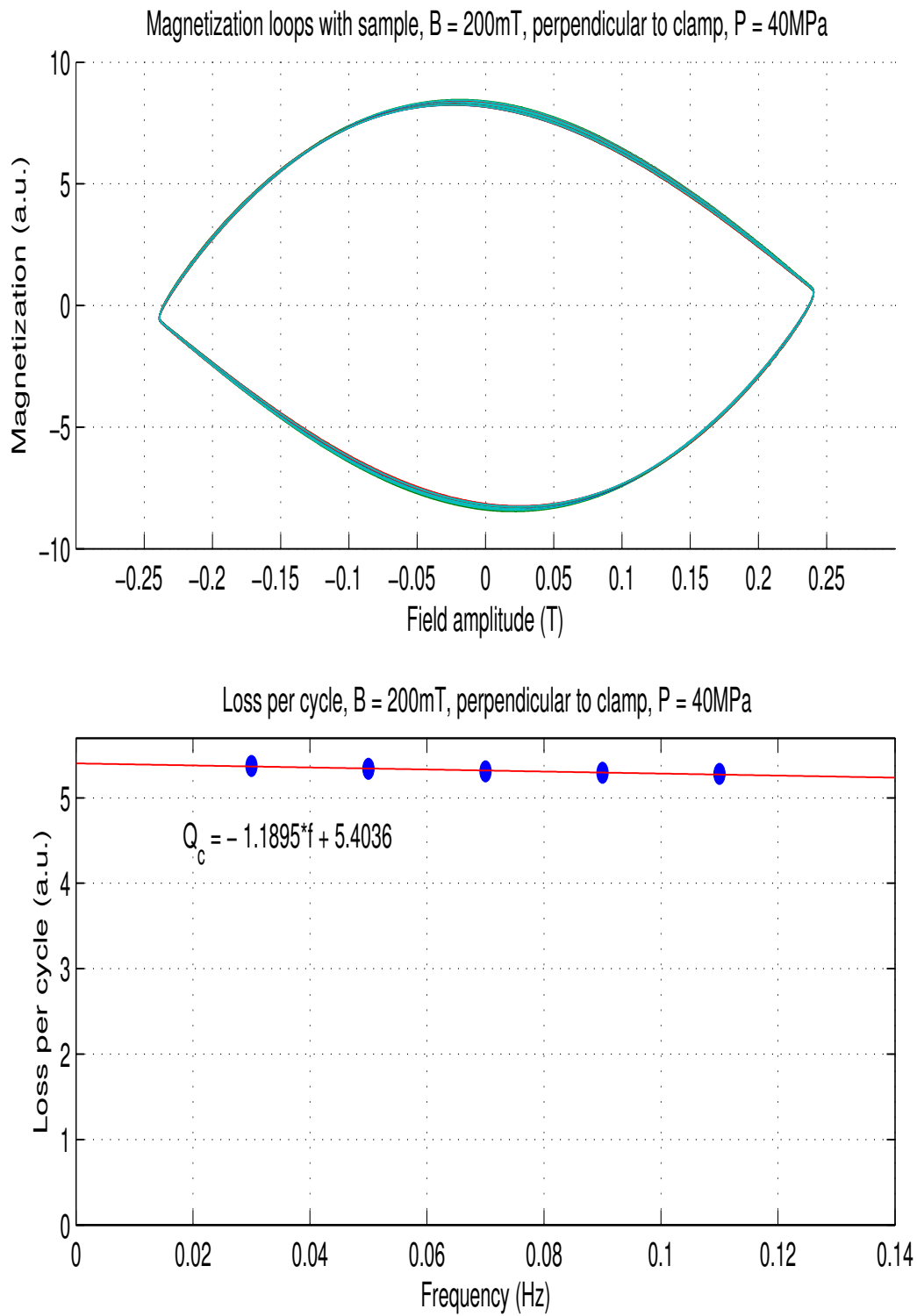


Figure B.11: *Top*: M(H) loops for each frequency (inner loop corresponding with the lowest frequency) and *Bottom*: loss per cycle  $Q_c(f)$  measured with the sample in a 200mT field, perpendicular to the clamp and 40MPa pressure.

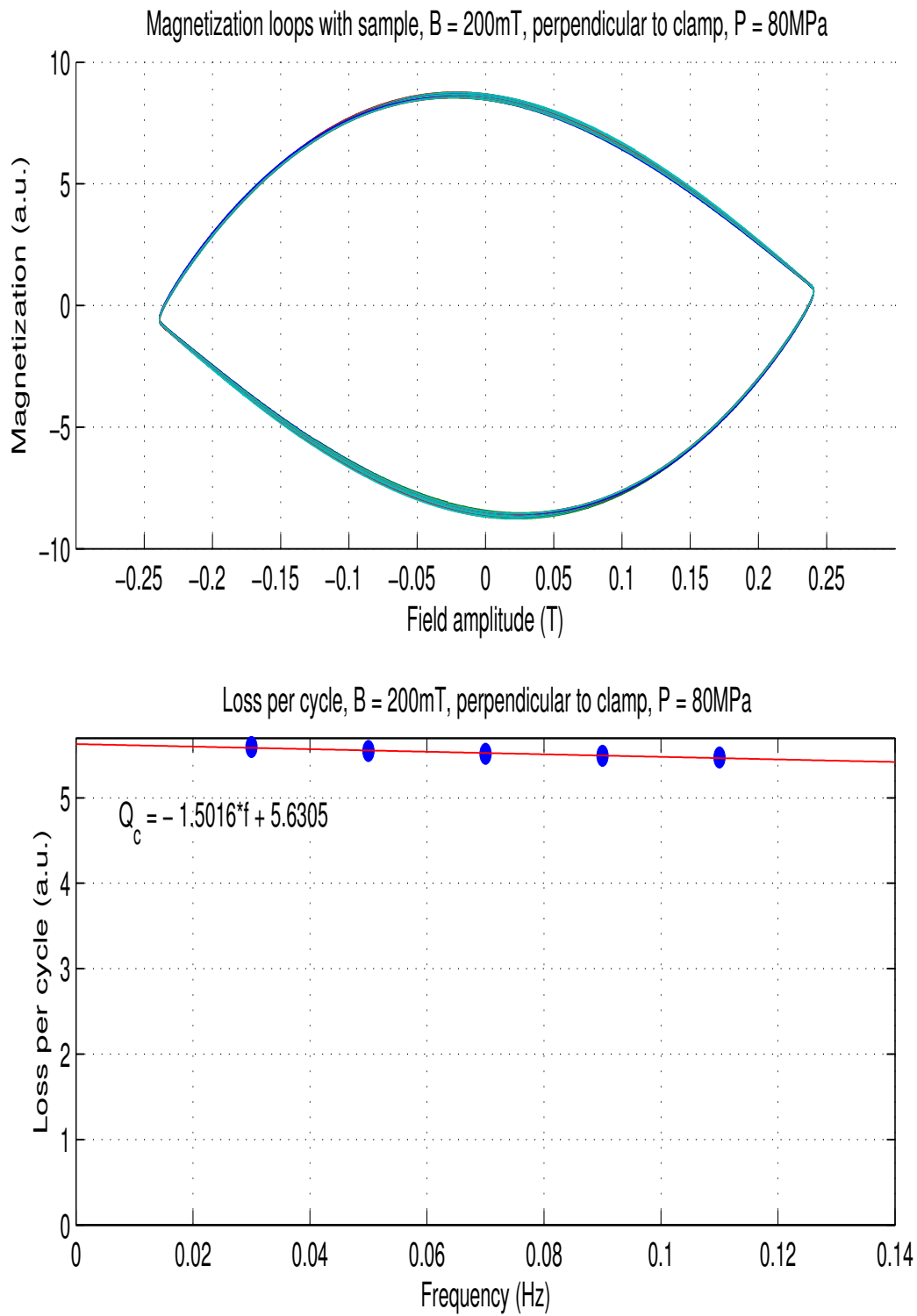


Figure B.12: *Top*: M(H) loops for each frequency (inner loop corresponding with the lowest frequency) and *Bottom*: loss per cycle  $Q_c(f)$  measured with the sample in a 200mT field, perpendicular to the clamp and 80MPa pressure.

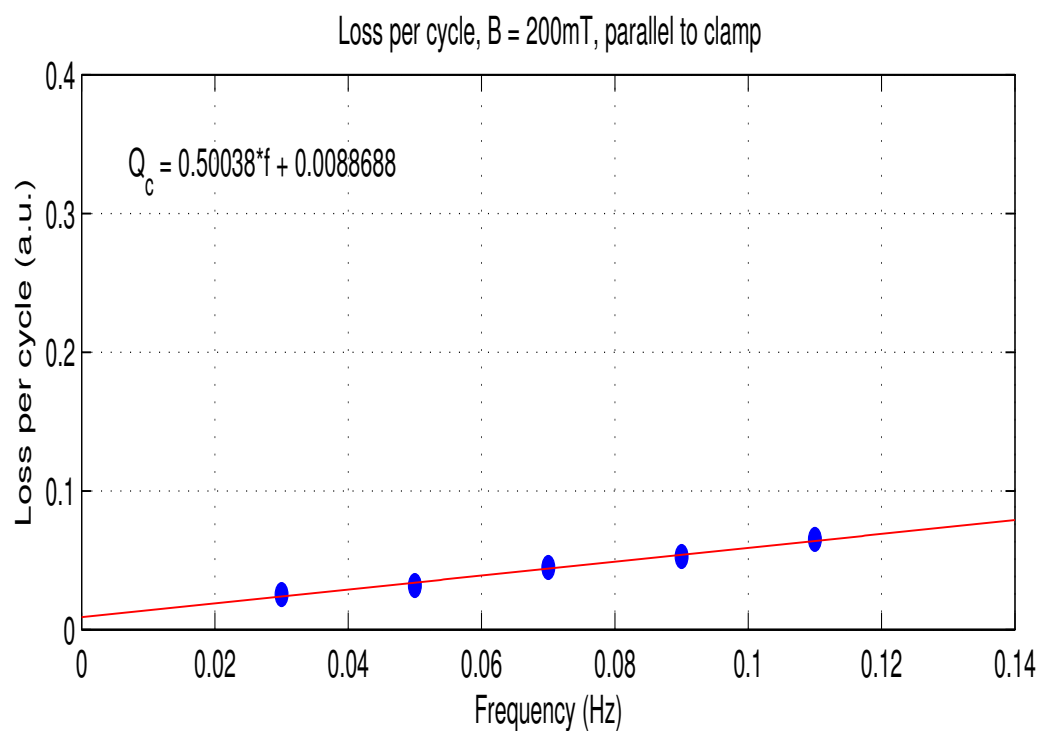
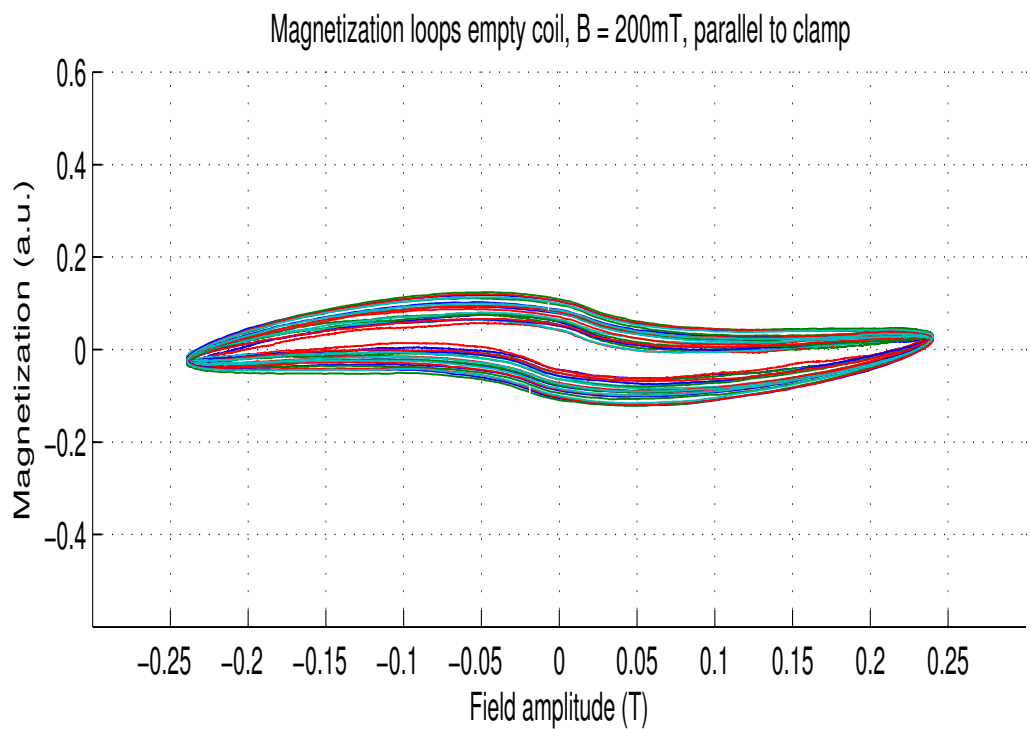


Figure B.13: *Top*: M(H) loops for each frequency (inner loop corresponding with the lowest frequency) and *Bottom*: loss per cycle  $Q_c(f)$  measured without the sample in a 200mT field, parallel to the clamp.

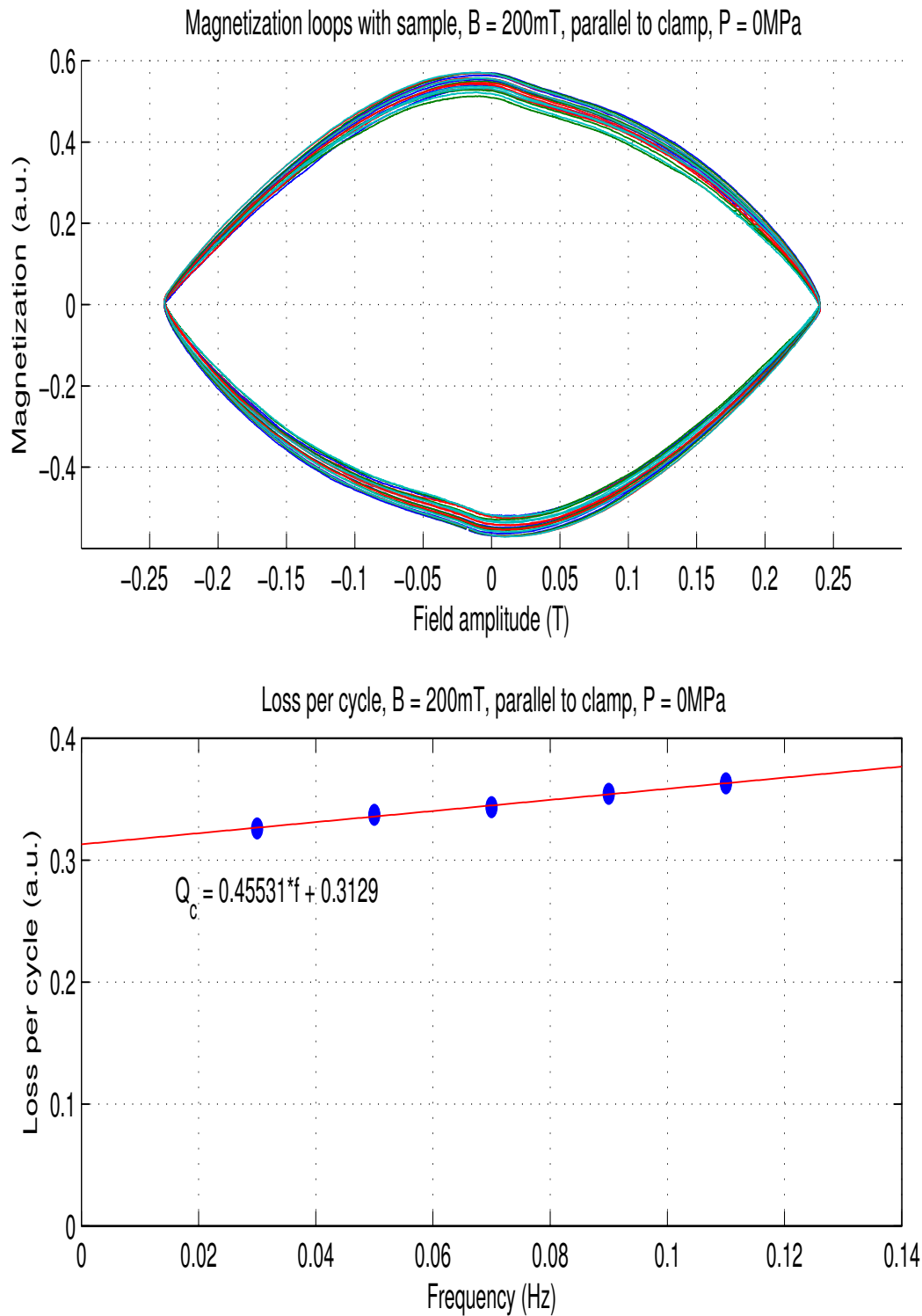


Figure B.14: *Top*: M(H) loops for each frequency (inner loop corresponding with the lowest frequency) and *Bottom*: loss per cycle  $Q_c(f)$  measured with the sample in a 200mT field, parallel to the clamp and no pressure.

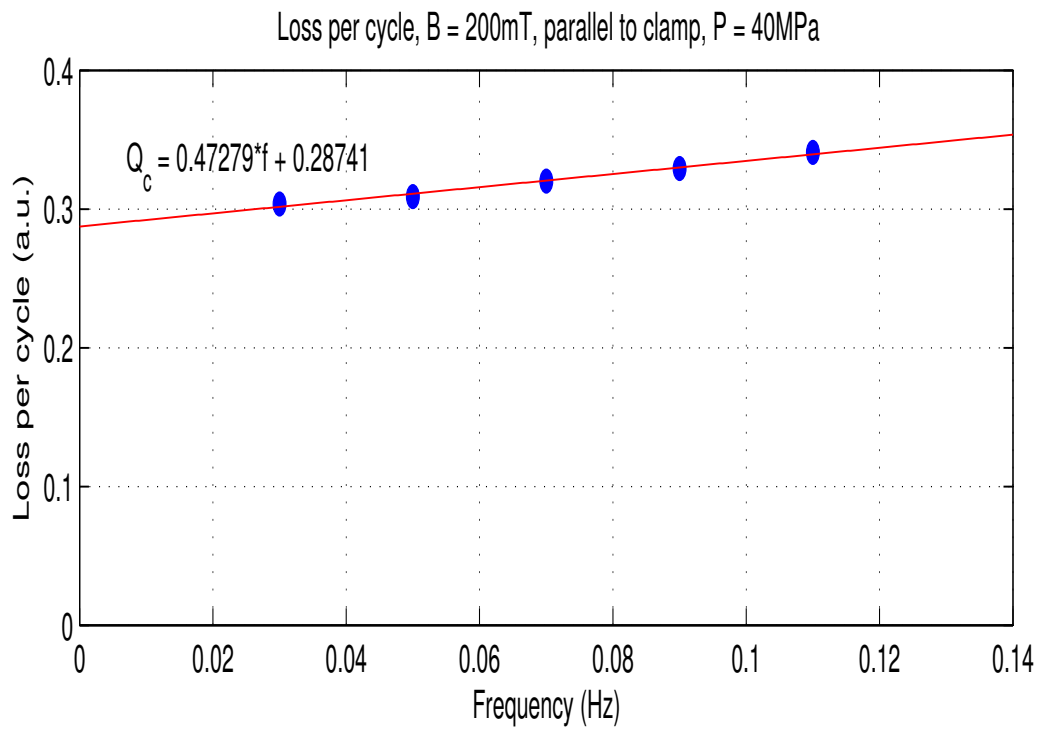
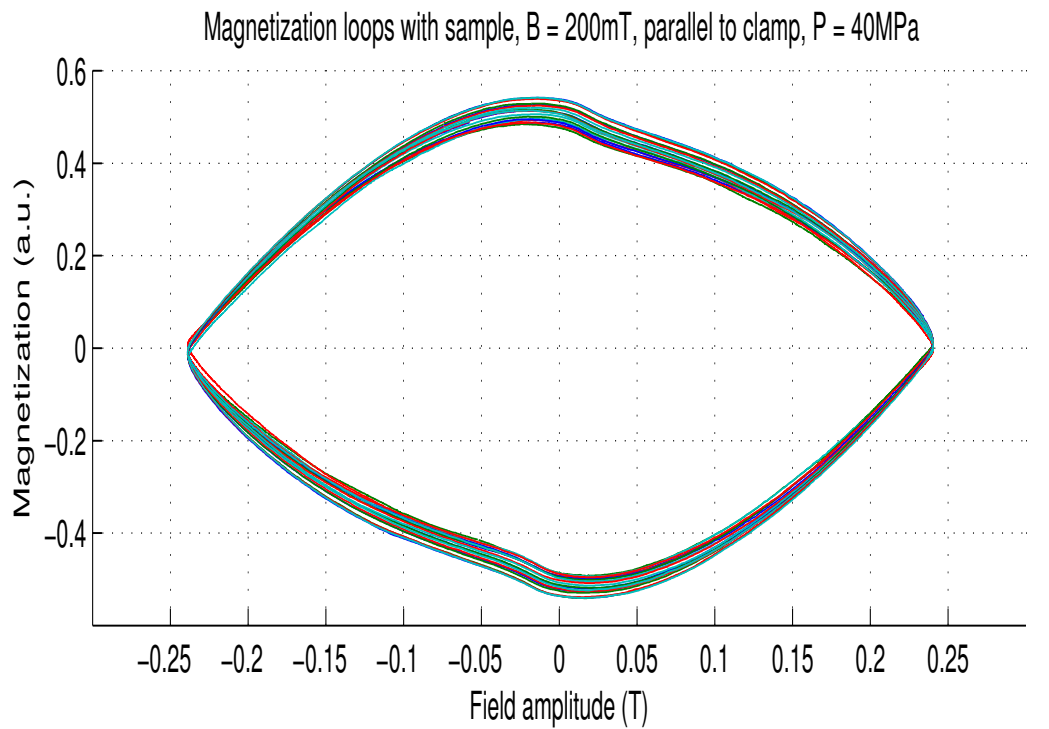


Figure B.15: *Top*: M(H) loops for each frequency (inner loop corresponding with the lowest frequency) and *Bottom*: loss per cycle  $Q_c(f)$  measured with the sample in a 200mT field, parallel to the clamp and 40MPa pressure.

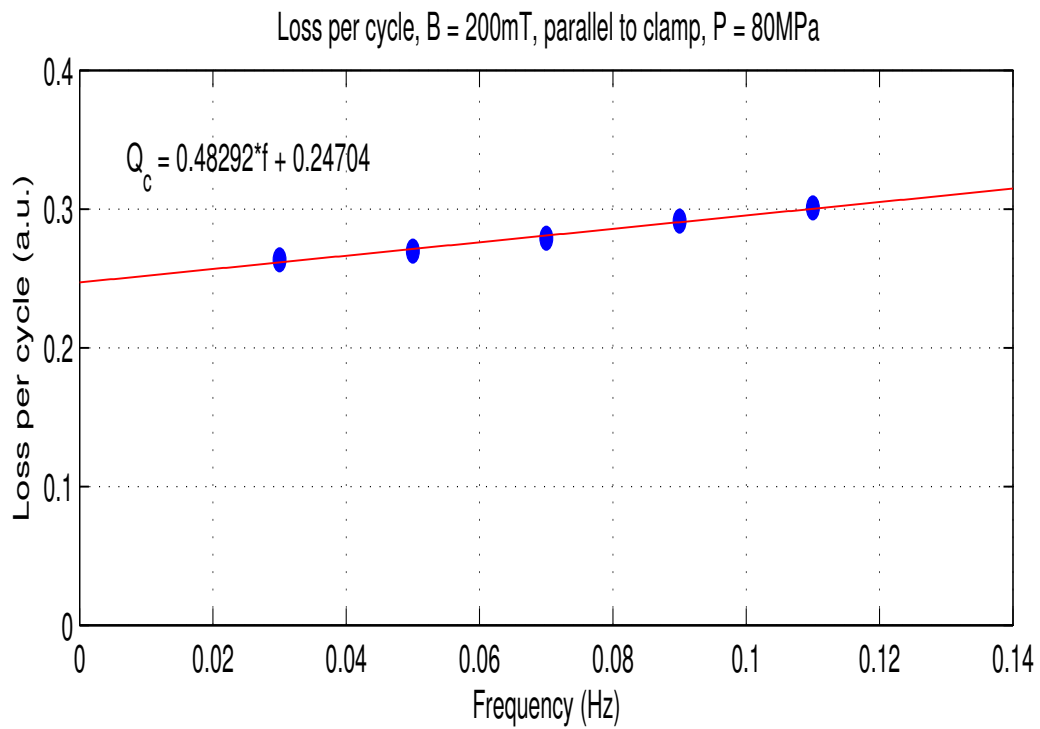
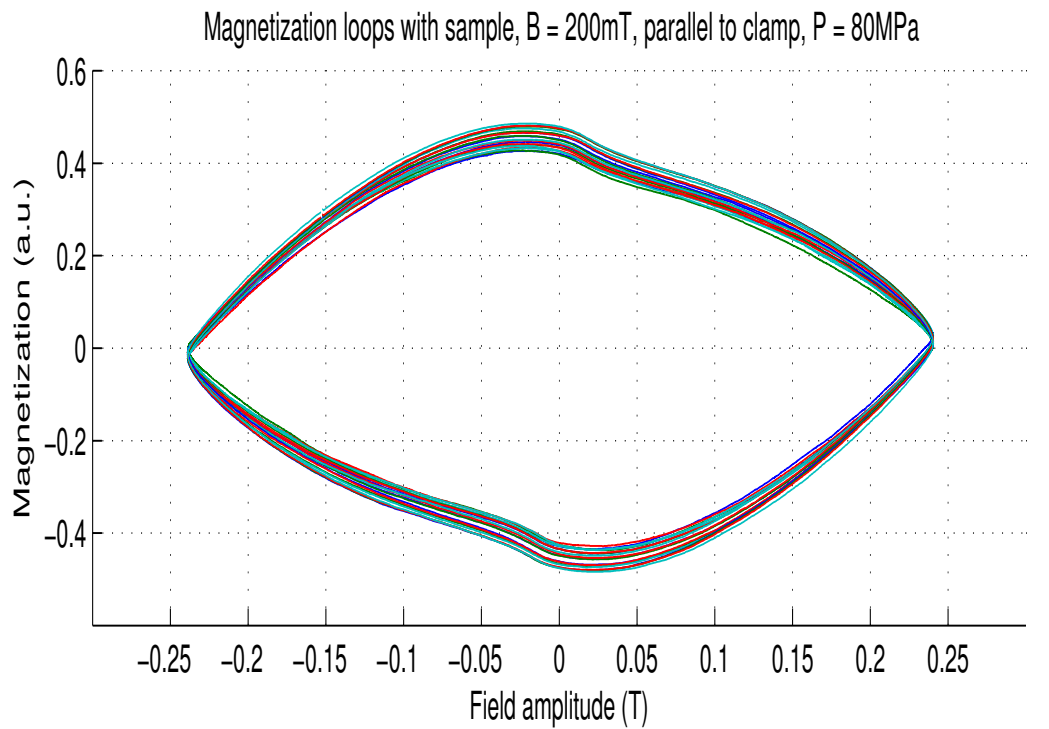


Figure B.16: *Top*: M(H) loops for each frequency (inner loop corresponding with the lowest frequency) and *Bottom*: loss per cycle  $Q_c(f)$  measured with the sample in a 200mT field, parallel to the clamp and 80MPa pressure.



## **APPENDIX C**

# **CLAMP PLATE CONSTRUCTION DRAWINGS**

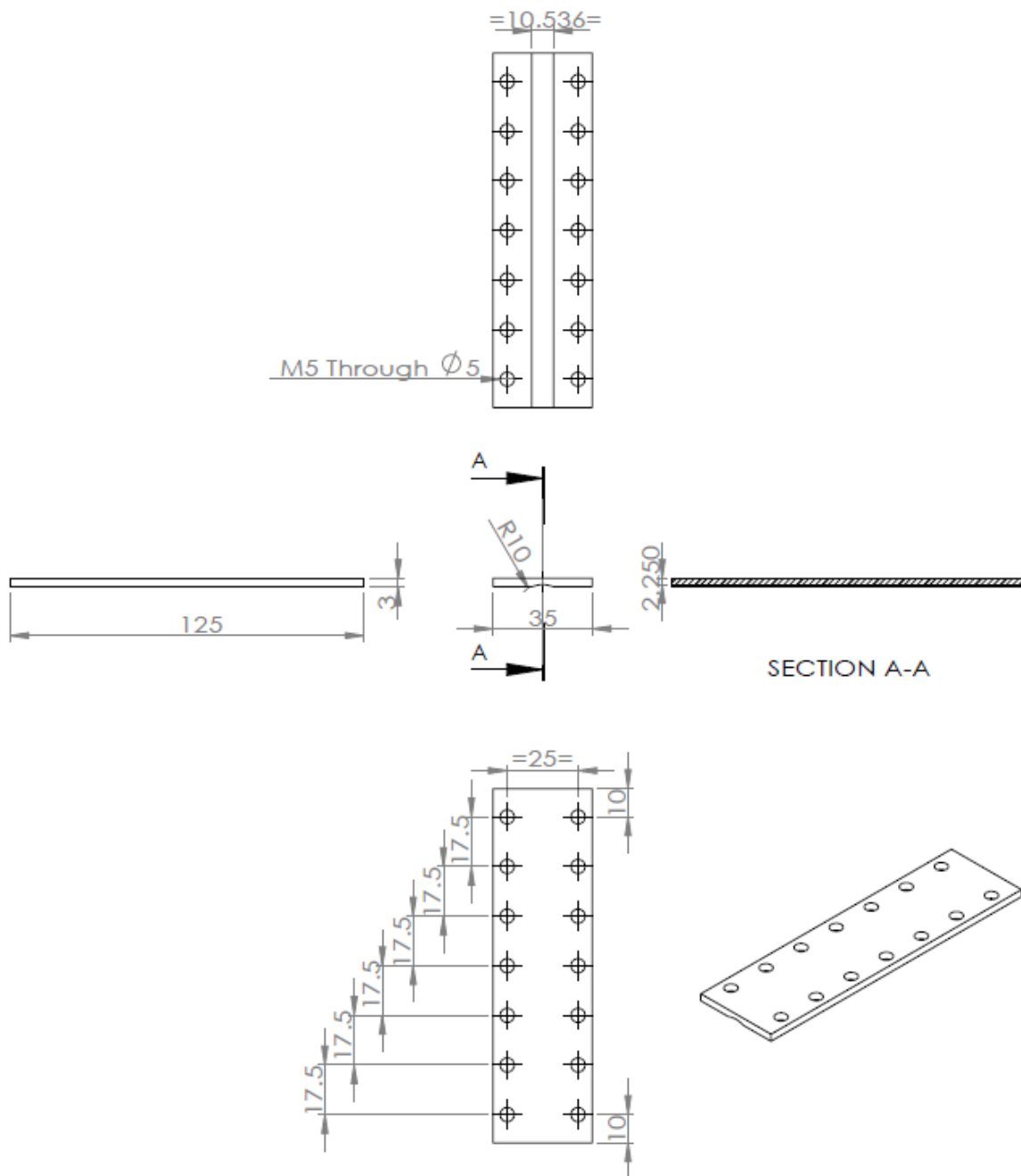


Figure C.1: The dimensions and layout of the clamp plate, all sizes are in mm.

# BIBLIOGRAPHY

- [1] C.W.G.D.M. Aarts et al, *Polytechnisch zakboekje*. PBNA.
- [2] L. Krempaský, A.C. *Losses in flat twisted superconducting cables*. European organization for nuclear research, 1978
- [3] M. N. Wilson, *Superconducting magnets*. Clarendon Press, Oxford University Press, 1983.
- [4] M. Parans Paranthaman, Teruo Izumi, *High-performance YBCO coated superconductor wires*. MRS Bulletin (august), 2004
- [5] M. Polak et al, *Frequency dependence of hysteresis loss in YBCO tapes*. Superconduct. Sci. Technol. 20 (S293-S298), 2007.
- [6] A. Wuis, *AC magnetisation loss: The roll of dimensionality*. Master thesis University of Twente, 2009.
- [7] Grilli et al, *Simulating Superconductors in AC Environment: Two Complementary COMSOL Models*. Excerpt from the Proceedings of the COMSOL Conference Milan, 2009.
- [8] J. Ridderbos, *Angular dependence of loss in YBCO sample with arbitrary field orientation*. Bachelor thesis University of Twente, 2009.
- [9] *High-temperature superconducting magnet cables reach a record current at a magnetic field of 20T*. Mag Lab Reports Vol. 19, no. 1, p. 9, 2012
- [10] H.H.J. ten Kate, M.M.J. Dhallé, *Lecture 1, 2 and 5 slides of 'Applications of Superconductivity'*. University of Twente, 2013.
- [11] Wikipedia, *Yttrium barium copper oxide*.
- [12] Wikipedia, *Bending*.
- [13] dr. M.M.J. Dhallé, *Private communication*.

